Inter-ply friction in unidirectional fiber-reinforced thermoplastics

With a focus on the influence of temperature

Thesis

I.J. Geschiere

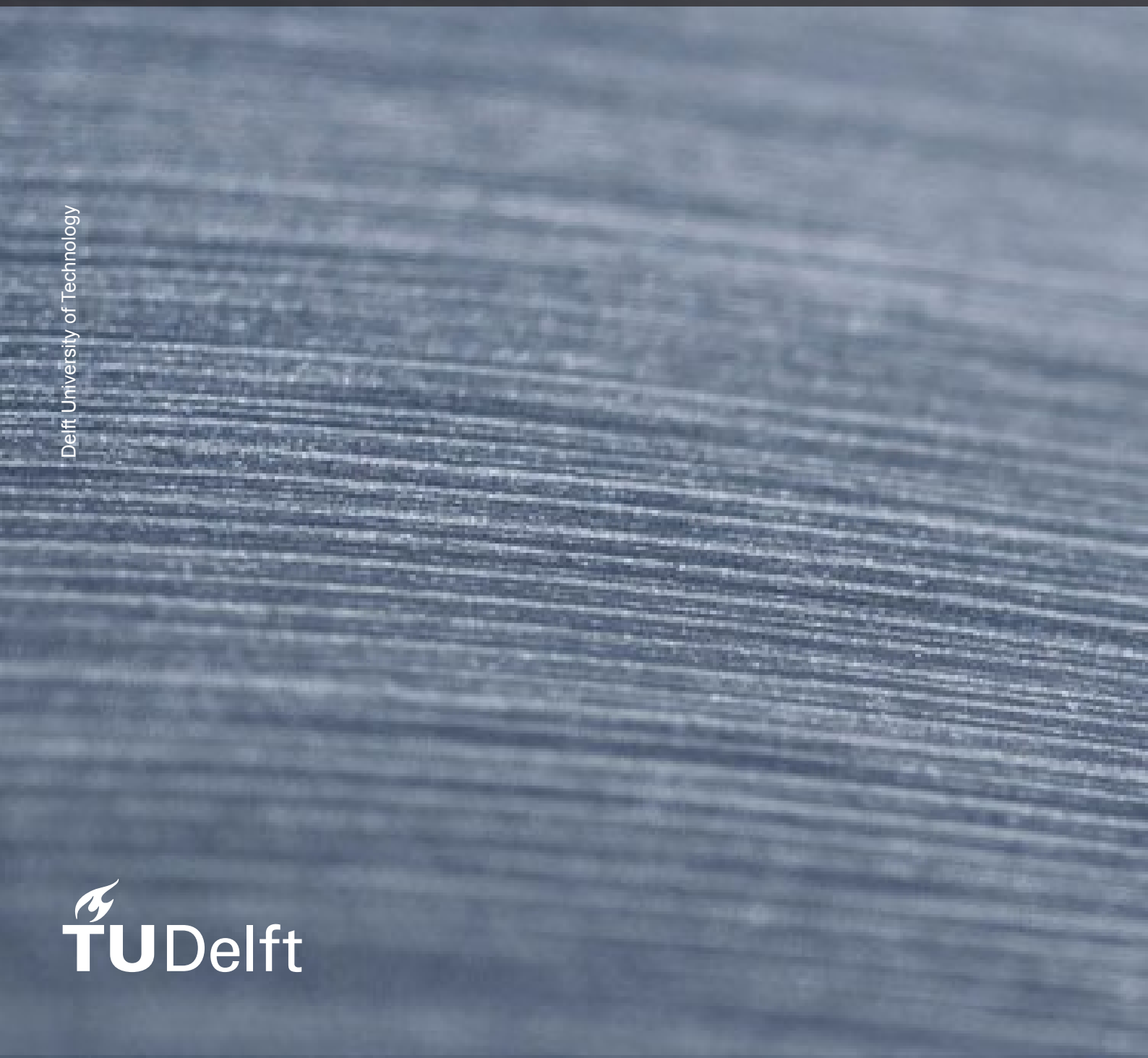

Delft University of Technology

TU Delft

Inter-ply friction in unidirectional fiber-reinforced thermoplastics

With a focus on the influence of temperature

by

I.J. Geschiere

Student number 5361524

University:	Delft University of Technology
Faculty:	Materials Science and Engineering
Research institution:	Thermoplastic composites research center
Supervisors TU Delft:	M.A. Bessa, J. Sinke
Supervisors TPRC:	E.R. Pierik, E.T.M. Krämer
Project Duration:	January, 2022 - October, 2022

Cover Image: Unidirectional prepreg C/PEEK (Toray Advanced Composites)

TU Delft

TPRC THERMOPLASTIC COMPOSITES RESEARCH CENTER

Preface

Before you lies the final product of my graduation research. With this report, I hope to conclude my time as a Materials Science and Engineering student at TU Delft. I have been a student for a little more than 6 years now. Almost half of this has not been the greatest of times because of the COVID-pandemic. Therefore, it has been an extra great pleasure to be able to leave my house every day again while graduating. I would like to thank the ThermoPlastic composites Research Center (TPRC) for the opportunity to work onsite with an interesting subject for the past 10 months. 10 Months in which I not only expanded my knowledge about thermoplastic composites and academic writing, I also learned that football can be quite tricky at times and that it is pretty blissful to use two hands for your daily tasks as a graduate.

Rens, thank you for the guidance on a daily basis, the coffee breaks together, answering my questions and lifting my academic skills to a higher level. I enjoyed our discussions during meetings and the joint efforts to increase the level of my report, all while being cheerful and patient. Erik, thanks for joining our discussions, giving your opinion on matters and of course for inviting me to graduate at TPRC in the first place. Graduating in a city more than 200 km away from your university might not be the most common situation. Therefore I would like to thank Jos and Miguel for their willingness to do all of our meetings online. But besides that, thanks for being my supervisor and aiding me with advice regarding graduation.

At last, I want to thank the other students and the technicians at TPRC who not only helped me with all of my questions and problems but also provided amusement on a daily basis.

I.J. Geschiere
Enschede, October 2022

Abstract

The accuracy of hot press forming process simulations with unidirectional fiber reinforced thermoplastics is not at the desired level. Fundamental knowledge about the interactions between adjacent plies is needed to enhance predictive quality. Several mechanisms can be distinguished during hot press forming of composites. This thesis focuses on the inter-ply friction behaviour which is the resistance against inter-ply slip. The main variable investigated in this study is temperature.

In this research, an extensive friction characterization with UD C/LM-PAEK is conducted at temperatures ranging from 300 to 365 °C. The neat matrix material has been studied with DSC and rheometry experiments. In general, a peak response can be seen during start-up in a friction characterization experiment. This peak, or overshoot, progresses towards a steady state friction response after a slip distance of several mm. Reducing the temperature showed similar effects to increasing the sliding velocity in a ply-ply slip system. The peak during start-up increases in magnitude while the steady state response remains approximately constant. Indications of flow induced crystallisation have been observed during friction characterization around the melting point of the material. The time-temperature-superposition principle has been applied to experimental friction data. This enabled to predict the duration of the transition of peak friction response towards a steady state. Several modelling efforts have been compared to the experimental data. The accuracy of the model predictions is similar between 315 and 365 °C. Influences of flow induced crystallisation impede the reliability of the specific models around and below the melting point.

The research lead to useful insights in the friction behaviour at relatively low temperatures. Further research is required on the field of flow induced crystallisation for a better understanding of its role in the friction response. Further study with other materials is needed to validate the application of the time-temperature-superposition principle to predict the speed of the transition of peak friction response towards steady state.

Keywords: Friction, Thermoplastic composites, Temperature, Hot press forming

Contents

Nomenclature

Abbreviations

Abbreviation	Definition
CFRT	Carbon fiber reinforced thermoplastic
COF	Coefficient of friction
FIC	Flow induced crystallisation
G	Glass fiber
C	Carbon fiber
IR	Infrared
LM-PAEK	Low melting polyaryletherketone
PA-6	Polyamide-6
PEEK	Polyetheretherketone
PP	Polypropylene
TTS	Time-temperature-superposition
UD	Unidirectional
WA-XRD	Wide angle X-ray diffraction

Symbols

Symbol	Definition	Unit
A^{visc}	Sliding surface in contact with polymer	m^2
a_T	Temperature shift factor	-
d	Max. displacement in pull-through test	m
E	Activation energy	J/mol
F	Pull force	N
F_f^{visc}	Viscous contribution friction force	N
F_N	Normal force	N
G'	Storage modulus	Pa
G''	Loss modulus	Pa
N	Normal force	N
H	Hersey number	m^{-1}
h	Matrix interlayer thickness	m
n	Power law index	-
R	Universal gas constant	$\text{J}/(\text{K}\cdot\text{mol})$
t_s	Shear duration	s
T	Temperature	K
T_ref	Reference temperature	K
U	Displacement	m
V	Sliding velocity	m/s
W	Specific work	J/m^3
w	Width of composite ply	m
δ	Phase shift angle	°
η	Viscosity	$\text{Pa}\cdot\text{s}$
η_0	Zero shear viscosity	$\text{Pa}\cdot\text{s}$
$\dot{\gamma}$	Shear rate	s^{-1}
γ	Shear	-

Symbol	Definition	Unit
μ	Friction coefficient	-
τ	Shear stress	Pa
τ^{crit}	Critical shear stress wall slip	Pa
τ^{visc}	Viscous shear stress	Pa
τ_{avg}	Average shear stress	Pa
τ^*	Critical shear stress (Cross model)	Pa

List of Figures

List of Tables

1 Introduction

Throughout the last century, an increase in the application of composites as a material for components in the aerospace industry has been accomplished. The applicability of composites in this industry is broad. One-third of the total weight of military aircraft consists of composite materials ranging from structural components to wings, fins and the radome [1]. The application is still limited in civil aviation but the applicability is increasing every year [1]. An example of this is the application of composites in primary structures, such as the wings and fuselage, of the Airbus A380 [2]. The innovation of these relatively new materials has not stopped after implementation. At first, the goal was to reduce the weight of an aircraft and therefore save fuel and costs. Nowadays the environmental footprint of the material itself is a hot topic. This is why it becomes of interest to use a fiber-reinforced thermoplastic rather than the conventional thermoset resin. The main advantage of thermoplastics is that they can be re-melted and re-shaped. Recycling of thermosets is more complex since it cannot be remelted [3]. But besides a relatively easier recycling process for thermoplastic composites, the initial production process can also be more efficient in terms of automation, costs, energy, and time.

Thermoplastic composite parts are traditionally produced by autoclave molding. With the autoclave molding technique, pre-impregnated woven fiber fabric or unidirectional (UD) tape is placed on a mold. Pre-impregnated tape means that thermoplastic matrix material is already present and equally distributed between the fibers. After the layup of composite plies is secured by a vacuum bag, the part is consolidated in the autoclave by exposing it to a specific pressure and temperature cycle. This production method is functional, but it is not efficient regarding production time, energy, and space [4].

It is for this reason that at the end of the 20th century, one started looking for alternatives. This led to the development of the hot press forming process. It can only be used with a thermoplastic matrix material because the material needs to be re-melted and reshaped. The main difference here is that the pressure onto the composite laminate is no longer hydrostatic but mechanically induced by a mold press. This same press is also used to push the composite laminate into its final shape using a male and female tool. A pre-consolidated composite blank is first heated to melt the matrix material, before being transferred to the mold press [5]. This process is faster and more cost-efficient than conventional autoclave molding but also the automation possibilities are more extensive [6, 7].

1.1. Aim of the study

A lot of research has been conducted about the hot press forming of woven fabric-reinforced thermoplastic composites [8, 9, 10, 11]. But UD oriented fibers offer new possibilities regarding automatic tape placement and thickness and layup variations. Also, higher fiber volume fractions can be achieved by using UD pre-impregnated tapes rather than pre-impregnated woven fabrics. Hence, a trend towards UD fiber-reinforced thermoplastics is visible in the industry [12].

However, greater formability issues are experienced when using UD tapes in hot press forming [5].

Where the complexity of part geometry goes up, so does the number of defects and issues in the produced parts. The most common issues are (related to) wrinkling and folding of the different plies in the laminate, see Figure 1.1. Such defects can lead to a mechanical deterioration of the final product by lack of consolidation or fiber waviness in defect areas [5]. Therefore, there is an urgent need for a better understanding of the forming behavior of UD pre-impregnated tapes during hot press forming. With this, accurate characterization and models can be realized and applied in simulation software. Simulations are a more efficient and cheaper method compared to experimental trial and error. An example of such software is Aniform [13], which utilizes a finite element method to simulate the hot press forming process. This research can be useful in the determination of input parameters or a subroutine regarding ply-ply friction modeling with respect to temperature. With this, prospective simulation-based designing can be used to prevent defects from occurring during actual production.

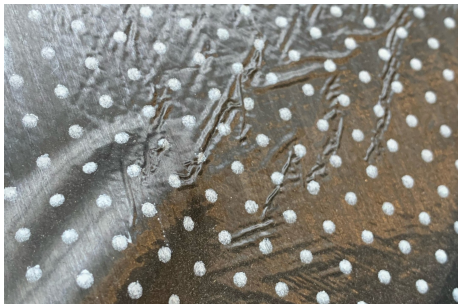

Figure 1.1: Wrinkles in a UD thermoplastic composite part.

There are specific deformation mechanisms during hot press forming that allow the composite laminate to be pressed into its final shape. These mechanisms occur within a single ply, as well as between adjacent plies. The former is called intra-ply and the latter is called inter-ply deformation. The intra-ply deformation mechanism consists of bending and shearing. The inter-ply deformation mechanisms are slip between adjacent plies and slip between the press or tool, and surface plies. This is called ply-ply slip and tool-ply slip. A delicate balance between these deformation mechanisms is what affects the formability of the material to form a defect-free part [14].

Several studies dealt with the slip behavior at the most common processing temperatures [5, 15, 16, 17, 18, 19, 20]. However, the tool is at a lower temperature compared to the composite laminate the forming stage. Therefore, it is also of interest to look into ply-ply friction at a lower temperature region as well. Since the material properties of the polymer are strongly influenced by temperature, it is expected that this has large consequences for the ply-ply slip behavior [5, 11, 21, 22]. In this research, the ply-ply friction, or resistance against slip, of UD fiber reinforced thermoplastics will be studied. The friction behavior will be characterized between the melting temperature and the typical processing temperature of the thermoplastic material. The main goal of this thesis is to obtain a better understanding of this behavior to predict forming defects during hot press forming more accurately. The goal can be expressed as a main research question in the form:

- *What is the effect of temperature on inter-ply friction of UD fiber-reinforced thermoplastics?*

Consisting of the following three sub-questions:

- *What is the effect of temperature on experimental friction characterization of UD fiber-reinforced thermoplastics?*
- *How do temperature effects in the neat matrix material relate to the experimental friction characterization results?*
- *What are the consequences for modeling and predicting frictional behavior of UD fiber-reinforced thermoplastics in a temperature window lower than the typical processing temperature?*

1.2. Structure

In this thesis, a literature review of studies related to friction in UD fiber-reinforced thermoplastics will be presented first, hereafter the remaining gaps will be outlined. The research is mostly based on ex-

perimental work, which can be divided into three different categories: thermal analysis, rheometry and friction characterization. First, the experimental method for all three different experiments is presented. Besides the experimental work, a model has been developed to predict part of the friction response, which is explained together with two existing models. The results from the models are compared to the obtained experimental data to assess their accuracy. The results from each of the experiments are given in the results section. The results are discussed and all information is combined in an attempt to fill the gaps in literature. A critical view of the study is outlined in the discussion and recommendations for further research are given. To finalize the report, the obtained knowledge is summarized in a conclusion. This conclusion can serve to fill the literature gap presented in the Literature Review.

2

Literature review

Hot press forming and the advantages over conventional autoclave molding have been briefly discussed in Chapter 1. In this section, a full outline of the process will be given along with several process parameters. The temperature cycle during the process and the deformation mechanisms that are enabling the forming of the composite are further explained. The general friction response will be discussed and the influence of the process parameters is outlined. Crystallization of the thermoplastic matrix material is related to friction characterization. At last, four different approaches to modeling the friction response in fiber-reinforced thermoplastics are explained and compared.

2.1. The hot press forming process

2.1.1. Pre-consolidation

UD plies are first pre-consolidated to obtain a laminate to use in a hot press forming process cycle. For this, one needs a layup of separate composite plies or UD tapes. The UD tapes are stacked on top of each other, each tape oriented in a specific prescribed direction to obtain a laminate with high strength in the desired directions. See Figure 2.1a for an example of such a layup.

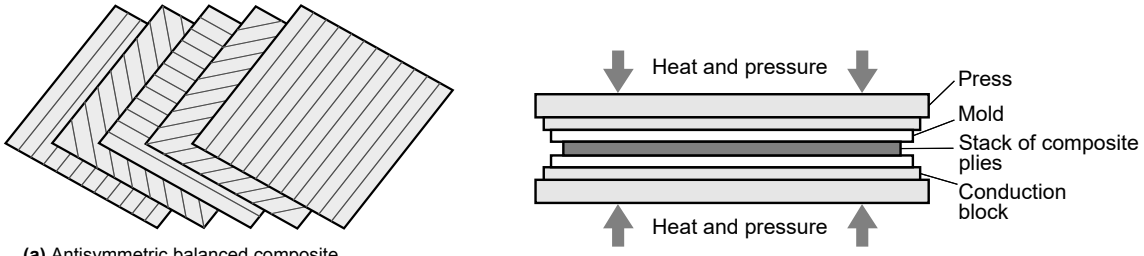

(a) Antisymmetric balanced composite laminate in layup (0°/-45°/90°/45°/0°). The lines displayed in each ply represent the fiber direction.

(b) Hot press pre-consolidation.

Figure 2.1: Schematic overview of stack of plies in antisymmetric layup and hot press pre-consolidation of thermoplastic composite laminate.

This stack of plies is then placed in either an autoclave or a press for the pre-consolidation process. A schematic overview of pre-consolidation using a heated press can be seen in Figure 2.1b. Pressure and temperature are needed to transform the separate plies into a firm solid composite laminate. The plies are flattened out during this process by the pressure and elevated temperature [23]. Also, a more homogeneous fiber volume fraction throughout the laminate is obtained [24].

When the laminate has consolidated properly, a bond is established between the separate plies. Overall, the quality of this bond and the composite laminate is determined by void formation during the consolidation process [25]. These voids can be formed by an insufficient extraction of volatiles. Other

examples of possible defects are fiber waviness, wrinkling or undulation [26]. The pre-consolidated laminates are subsequently used as starting point for the hot press forming process.

A typical temperature and pressure versus time profile for a UD thermoplastic laminate during hot press pre-consolidation is given in Figure 2.2. At first, the pressure is relatively low and stable, while the temperature is gradually increasing up to the processing temperature. Shortly after reaching the processing temperature, the laminate is further compressed by an instantaneous pressure increase. After a dwell time of approximately 40 minutes, the laminate is cooled down again while maintaining the high pressure [27]. After this final step, the laminate has consolidated properly and it should be void-free at the ply interfaces.

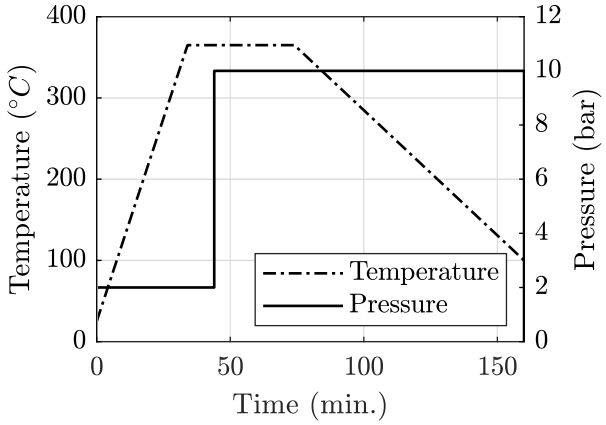

Figure 2.2: Typical pressure and temperature profile for UD thermoplastic composite laminate during press pre-consolidation [27].

2.1.2. Hot press forming

The actual forming process contains four different steps: heating, positioning, forming and consolidation & cooling. This is also illustrated in Figure 2.3.

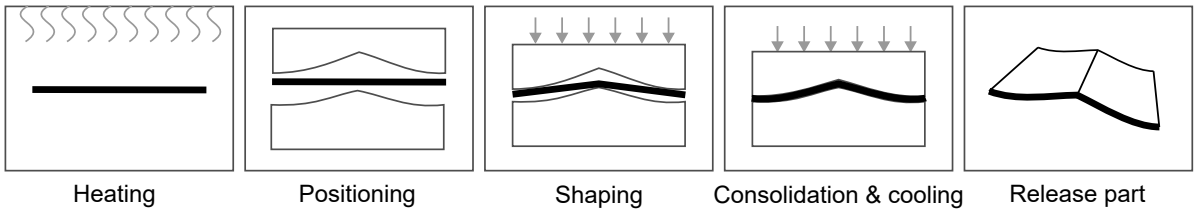

Figure 2.3: Stepwise illustration of hot press forming process.

The pre-consolidated laminate already has the desired holes and varying thicknesses in combination with a suitable layup. The laminate can be clamped at the edges and is heated by infrared (IR) radiation to the specific process temperature. This temperature is dependent on the thermoplastic material. The hot laminate is transported to the optimal position between the male and female press tools after reaching the desired temperature. The transport has to be as quick as possible to minimize heat loss. The male and female tools are clamped together to shape the blank into the desired geometry during the forming stage.

The tools are at a specific temperature between the glass and melting temperature of the used thermoplastic [28]. The severity of the part cooling can be controlled this way to optimize the crystallization process. The cooling process is initiated immediately after the part touches the tool. This means that shaping and cooling are partially simultaneous processes. After the part has been pressed in the right

shape, the tool still presses it together for a few more seconds. The consolidation along with the remaining cooling takes place during this step. The male and female tools are opened again after complete cooling and the part is released. Finishing steps, such as cutting away the flange, are needed before the product is ready to use.

The temperature of a composite part during hot press forming is visualized schematically in Figure 2.4, showing a typical temperature curve during hot press forming of a C/LM-PAEK composite blank [27]. Phase III and IV is the time under pressure of the tool. It can be seen that the temperature of the blank rapidly drops from the processing temperature (T_p) to the tool temperature (T_t) after the tool closes. The entire process has a duration in the order of minutes. More details about the temperature inside the material during the forming stage will be given in Section 2.5.5.

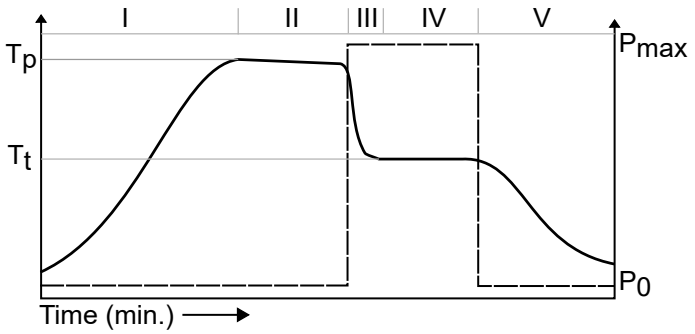

Figure 2.4: Typical temperature and pressure profile during hot press forming [27]. I: heating, II: transport, III: shaping, IV: consolidation, V: cooling and release. T_p is the processing temperature of the material, T_t is the tool temperature. Constant pressure is applied by the press/mold on the laminate during the shaping and consolidation stage.

2.2. Deformation mechanisms

As mentioned before in Chapter 1, different deformation mechanisms are active in the laminate during hot press forming. Tool-ply and ply-ply slip are the most important concerning the subject of this thesis. They will be discussed extensively in this literature review. The other mechanisms will also be explained for a general understanding of the process, namely intra-ply shearing, bending of plies and transverse squeeze flow [9].

2.2.1. Intra-ply shearing

Intra-ply shearing of UD composites is defined as the parallel movement of fibers. This can occur in-plane, but also in the through-thickness transverse plane [29]. This is best explained by the illustration in Figure 2.5. Here the three different intra-ply shearing modes are given. When a laminate consisting of multiple plies is sheared, it is likely that inter-ply slip occurs. But intra-ply shear is the shearing of a single ply and thus does not include the motion by slip.

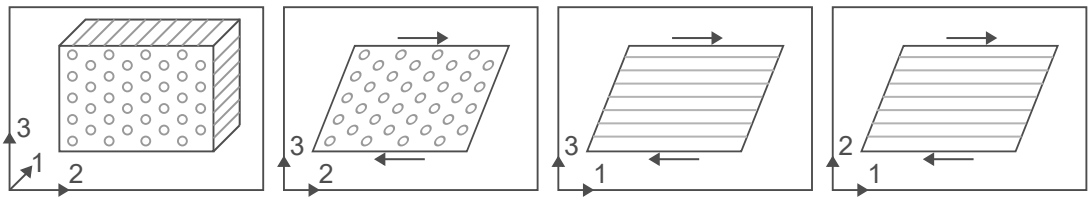

Figure 2.5: Intra-ply shearing of UD plies. 1 is the fiber direction, 2 is the in-plane direction normal to the fibers and 3 is the out-of-plane direction. From 2$^{\mathrm{nd}}$ to 4$^{\mathrm{th}}$: transverse shearing, longitudinal shearing, in-plane shearing.

2.2.2. Bending

Another deformation mechanism in hot press forming is bending of multiple plies. It can be found in geometries with a single or double curvature. It has been extensively studied, the mechanism can be modeled as layers of elastic fibers with a viscous polymeric material in between the layers [5]. The mechanism is illustrated in Figure 2.6a. From this illustration, it becomes clear that several different mechanisms are linked to each other. To bend multiple plies, they have to slip on the interface, which is ply-ply slip.

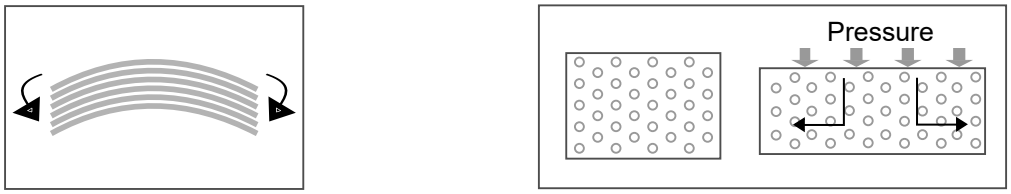

(a) Bending of a stack of composite plies.

(b) Transverse squeeze flow in a UD ply due to a normal pressure. Matrix-rich regions are formed on the sides.

Figure 2.6: The bending and transverse squeeze flow deformation mechanism in thermoplastic composite hot press forming.

2.2.3. Transverse squeeze flow

Transverse squeeze flow is a phenomenon that occurs mostly during consolidation. It can also occur during the forming stage but to a lesser extent. Transverse squeeze flow can be defined as the transverse movement of fibers due to a normal pressure. This is not possible in woven fabric, but only in UD composite material [30]. An illustration is given in Figure 2.6b. The phenomenon can be compared to the Poisson effect. However, the material is not stretching in the transversal direction when a normal pressure is applied, but it can be regarded as a flow of material from one place to the other. This means that it is only possible above the melting point of the matrix material.

2.2.4. Slip

Ply-ply and tool-ply slip are linked to almost any deformation mechanism described above. Slip and friction are antagonists, one can see friction as the resistance against slip. Slip is here defined as the in-plane movement of complete plies relative to another, see Figure 2.7, which occurs in both UD and fabric-based composites. Ply-ply slip is a complex phenomenon because multiple materials are involved in the slip system. Observatory research is not possible since the ply-ply slip process is completely shielded during hot press forming. Moreover, all other deformation mechanisms have to be suppressed to accurately characterize only the slip or friction behavior. Characterization experiments have been developed for this reason. The goal is to mimic the slip during hot press forming and quantify the friction while doing so. More details on the ply-ply slip behavior and the characterization will be given in Section 2.3.

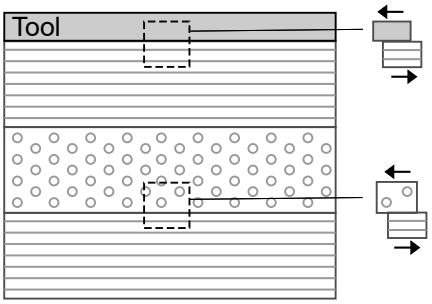

Figure 2.7: Ply-ply and tool-ply slip schematically illustrated.

The tool-ply slip is closely related to ply-ply slip. The difference is the materials of the two surfaces in contact. Where ply-ply slip occurs between the same materials, tool-ply slip is between a composite ply and a tooling surface. This tooling is in most situations made from either aluminum or rubber. Of course, the material also influences the tool-ply friction behavior. The presence of a mold release

agent has a relatively large influence on the tool-ply slip behavior [31]. Therefore, tool-ply friction is not characterized in this research, because the results would be highly influenced by the kind, amount and application method of the specific release agent. This increases the complexity of the slip system. A release agent is not applicable in ply-ply slip, which means that this is a phenomenon related to the specific composite material or its properties rather than a system problem. Hence, a fundamental understanding of the behavior is more important which is why the scope of this research is limited to ply-ply friction.

2.3. Friction in hot press forming

Over the past decades, several studies attempted to capture the friction behavior by use of experimental work. The different approaches will be discussed in this section. All discussed studies concern a composite with a thermoplastic matrix material with mostly a UD carbon fiber reinforcement. Also, some work about woven reinforcement is included because the amount of literature on friction in UD composites is limited.

The difference between ply-ply and tool-ply slip has already been discussed in Section 2.2.4. It can be seen throughout the literature that the resistance against slip, i.e. the friction, is not the same for both slip systems. However, it can be tested similarly. A first attempt to do this has been with a conventional plate-plate rheometer by Groves et al., who characterized inter-ply slip and intra-ply shear flow simultaneously [32]. The setup is displayed in Figure 2.8. A stack of plies is placed between the two plates before being heated to a specific temperature higher than the melting temperature. The stack of plies is subjected to oscillatory torsion by rotating the plates relative to each other. This way the dynamic viscosity could be related to a steady-state combination of intra-ply shear and inter-ply slip [5]. This immediately emphasizes the disadvantage of this method, the two different deformation mechanisms cannot be distinguished separately.

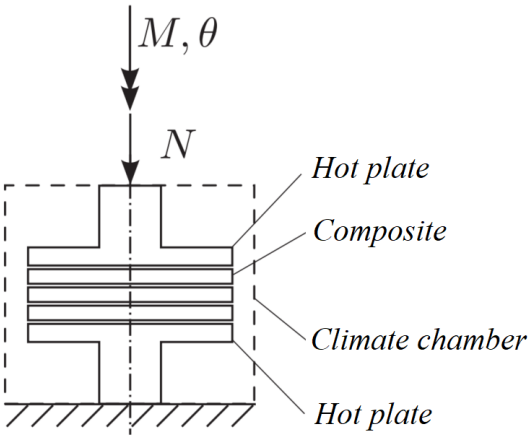

Figure 2.8: Oscillatory torsion deformation test method to characterize composite intra-ply shear and inter-ply slip by Groves [5, 32].

A new method has been developed to characterize the shear and slip in a more enhanced manner and it is used in multiple studies [17, 18, 22]. The method is illustrated in Figure 2.9. In this setup, a ply or sub-laminate is pulled from between two clamped surfaces. This is the so-called pull-out test. In between the pulled ply and the clamps can be another laminate with a specific fiber orientation [17] or a layer of tool-material [18], which is specifically illustrated in Figure 2.9b. The possibility to change the material at the slip interface makes it possible to characterize both ply-ply and tool-ply slip. The temperature in the composite material can be actively controlled by heating or cooling the clamps. Using the pull-out test, a larger influence by the orientation of the fibers can be distinguished than was possible with the oscillatory torsion method. More important, slip can be characterized isolated from the influence of intra-ply shear [5].

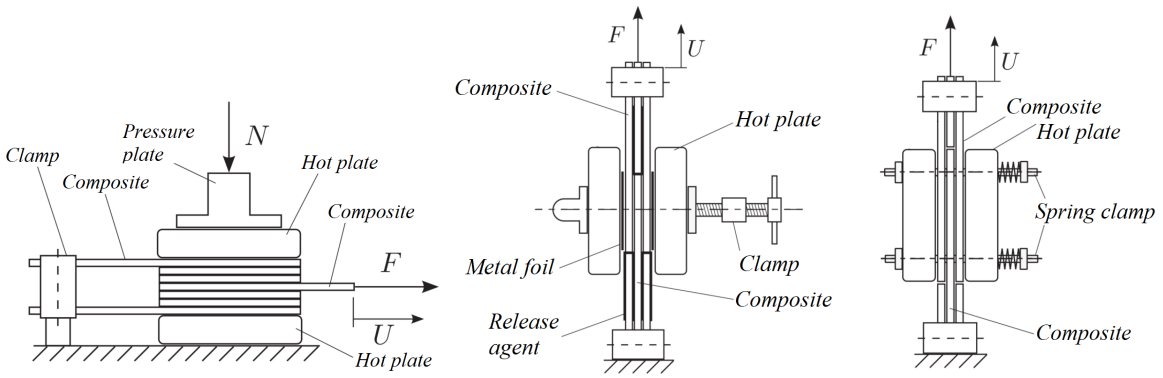

(a) Scherer and Friedrich [5, 22]. **(b)** Morris and Sun [5, 18]. **(c)** Lebrun [5, 17].

Figure 2.9: Different lab setups to characterize friction and slip behavior for composite plies or sublaminates, F is the required force to maintain the velocity during pulling, U is the displacement vector and N is the normal force [5].

$$\tau = \frac{F_{\text{pull}}}{2A} \tag{2.1}$$

In all test methods described in Figure 2.9, the pulled ply or sublaminate can be moved by a specific velocity. This velocity is the time derivative of the displacement (U). The required force to maintain this velocity is logged during the experiment, which can be converted to a shear stress present at the slip interface according to Equation 2.1. A represents the clamped surface area, multiplied by two because the ply or sublaminate has a slip interface on each side. This highlights the main disadvantage of a pull-out test. When the specimen slides through the clamps, the clamped surface area A will decrease causing a non-negligible normal pressure increase during testing [11].

To reduce the interference by intra-ply shear, a setup can be used where the fibers of all stationary composite layers are fixed, preventing any movement [19]. This setup can be seen in figure Figure 2.10a. Only tool-ply friction can be characterized with the displayed setup because a metal foil is being pulled from between two composite plies. Nevertheless, it is perceivable to substitute the metal foil for another composite ply with fibers oriented in the same direction as the displacement vector. This way it is possible to look into ply-ply friction as well and it is called the pull-through method.

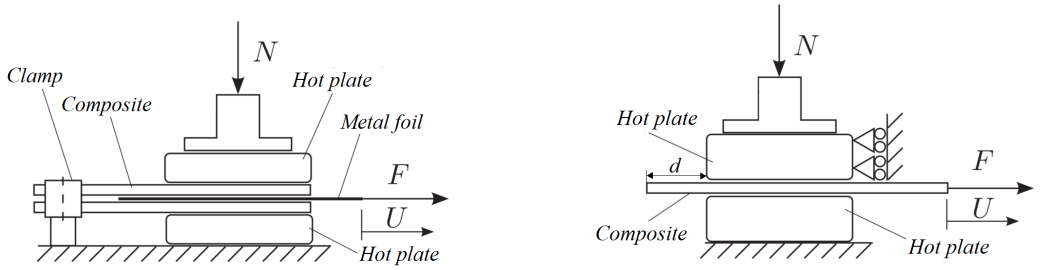

(a) Test setup used by Murtagh et. al with fibers fixated and a steel foil that is being pulled [5, 19]. **(b)** Pull-through test setup by Gorczyca et al. Maximum displacement possible is indicated by length d [5, 8, 16].

Figure 2.10: Two different test setups to characterize friction in composite laminate forming [5].

As mentioned before, the disadvantage of a pull-out test is the normal pressure inhomogeneity during testing. This can be prevented with a pull-through test rather than a pull-out test. The difference lies in the way how the ply is pulled from between the clamped system. The pulled ply is clamped on its entire surface in a pull-out test. This leads to a reduction of contact area while performing the test. In a pull-through test, the pulled ply has a surplus in length which is found at the side opposite to the pulled end. This extra length prevents a reduction of the clamped surface while testing. The pull-through test is at this moment the most used method to characterize inter-ply friction and it has been used in multiple

studies [8, 16]. An example of a pull-through test setup can be found in Figure 2.10b. The maximum displacement for a single test specimen is equal to the distance d in Figure 2.10b.

2.4. Typical friction response

The general friction characterization methods for thermoplastic composites are explained. The different testing methods lead to comparable responses. However, this response is dependent on process parameters such as normal pressure, temperature, velocity and fiber orientation. In this paragraph, the general friction response will be outlined. The influence of each parameter will be discussed in Section 2.5.

$$\mu = \frac{F_{\text{pull}}}{2 \cdot F_{\text{N}}} \tag{2.2}$$

In an isothermal test, with fixed normal pressure and velocity, a typical response looks like Figure 2.11. A clear peak and steady state region can be distinguished. The force (F_{pull}) needed to maintain the sliding velocity is already converted to a coefficient of friction (COF, μ) at the slip surface using Equation 2.2 [14]. By conversion to a COF, the friction is normalized for the applied normal pressure. The required pulling force can also be converted to a shear stress by dividing it by the two slip surfaces. During a pull-through test, the force can be logged while the velocity of the pulled ply is kept constant. In specific setups, it is also possible to log the displacement or velocity, while the force is kept constant. The driving force for slip is fixed in such a setup and the resulting velocity of the ply is logged. In such a situation it would be possible to investigate a static COF [33].

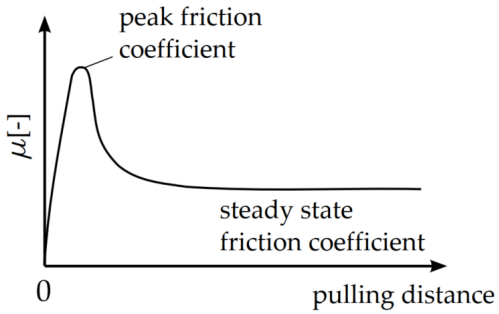

Figure 2.11: Schematic response of pull-out/pull-through experiments when one would consider the COF (μ) according to Equation 2.2. With a constant normal force, the curve for the pull force versus distance would be similar [14].

According to Lebrun et al. [17], the peak during start-up is caused by a static friction response. This would mean that the pulled ply is not slipping until the stress overcomes this static friction before evolving in a steady state friction response. This theory is comparable to Coulomb friction for dry surfaces where a static and a dynamic COF are used [33]. However, the friction characterization setup does measure a displacement during the start-up peak. It seems implausible that the measured displacement is caused by an elongation of the composite ply, considering the tensional stiffness of the fibers. It is more likely that the setup has a small slack or that the sample has slipped in the clamp rather than on the slip surface. This would be unique behavior for the specific setup, which would explain that the theory by Lebrun et al. [17] is not supported by other studies.

Murtagh and Mallon [19] proposed a different theory for the peak start-up behavior. They stated that during motion, the polymeric matrix material is percolating through the fibers in a transverse direction toward the sliding surface. During start-up, the matrix interlayer thickness would be thinner and it would increase due to this percolation. They also suggested that this extra resin material flows back to the bulk when the movement has stopped. However, they were not able to prove that it causes the initial peak force.

Morris and Sun [18] validated that the peak in the curve is not caused by irregularities in the testing equipment. It appeared that the peak was consistent throughout their measurements. To validate this, a test was conducted until the steady state was attained. The test was then stopped for at least 10 seconds and then restarted. Consequently, the same peak in shear stress was found immediately after the onset of slipping. This led to the conclusion that the peak shear stress had to be a specific yielding point in the mechanism. The results from the validation test by Morris and Sun can be seen in Figure 2.12. In this specific test, the sliding velocity is increased after the restart, causing the second peak to be higher. In similar tests with a constant velocity, the peaks were of identical height [18]. The yielding point theory was further investigated in later studies, where it was found to be the onset of strong wall slip at the fiber-matrix interface [5, 20].

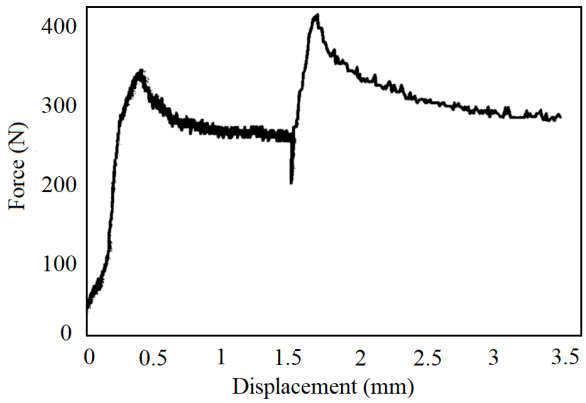

Figure 2.12: Validation of start-up behavior during friction testing. The force on the y-axis is the pulling force required to pull a single ply from a stack of plies in a pull-out test. The slipping velocity is increased at restart causing the second peak to be higher [18].

2.5. Parameters influencing friction behavior

The typical ply-ply friction response of a thermoplastic composite has been discussed in the previous section. However, this response is not identical in every situation. The influence on the friction response by several process parameters will be discussed in this section. The parameters that are considered most important are the normal pressure, the sliding velocity, the fiber orientation of the composite plies and the temperature of the laminate during friction characterization. Together, these parameters simulate the process during actual hot press forming. The location in a production cycle of hot press forming has a high influence on the temperature inside the laminate, which will be discussed separately.

2.5.1. Normal pressure

When relating normal pressure to the friction response, it is important to take note of the terminology. The normal pressure is the normal force divided by the slip surface of the ply. The shear stress response is the required pulling force divided by the same two slip surfaces. The COF is given according to Equation 2.2.

A representative analogy for a molten UD composite laminate is a wet towel. There is still in-plane tensional stiffness but the stiffness in all other directions is mostly gone. Consequently, the normal pressure on a laminate does not need to be very high to deform the laminate in the desired shape. The required force is mostly in the order of a thousand Newton, but it strongly depends on the geometry, layup and size of the part [19]. The inter-ply friction is dependent on the normal pressure, but this effect is different when looking at ply-ply or tool-ply friction systems. Both of the effects will be discussed separately.

Tool-ply effect
Several studies have investigated the influence of normal pressure on the tool-ply friction response. Murtagh et al. [19] investigated the shear stress response in UD AS4/PEEK when increasing the normal pressure. They reported an increase in the steady state tool-ply shear stress for relatively low sliding velocities (12 mm/min.). For higher sliding velocities (120 mm/min.), the steady state tool-ply shear stress stayed approximately the same. Gorczyca et al. [8] also reported an increase in the tool-ply shear stress when increasing the normal pressure with woven G/PP. However, it was not reported whether this only applied to the steady state tool-ply friction or if it also applied to the peak behavior. Ten Thije et al. [34] investigated the effect of normal pressure on both the peak and the steady state tool-ply friction for woven G/PP. Both peak and steady state tool-ply shear stress response increased with increasing normal pressure. The severity of the effect is larger in the work by Murtagh et al. [19], compared to the work by Gorzcyca et al. [8] and Ten Thije et al. [34]. This underlines the hypothesis that the effect is dependent on the fiber architecture of the composite.

Ply-ply effect
Murtagh and Mallon [35] investigated the ply-ply steady state shear stress for UD APC-2. They reported a doubled shear stress after increasing the normal pressure by a factor of four. All while keeping sliding velocity and temperature constant. Morris and Sun [18] looked into UD AS4/PEEK. They saw an increase in the steady state shear stress by approximately the same factor as they increased the normal pressure with. They attributed the effect of increasing shear stress to the transverse spreading of the molten matrix material, leading to dry spots inducing local normal pressure peaks [18]. In both studies, the distinction between peak and steady state response has not been made. The separate effects of normal pressure on peak and steady state behavior in ply-ply friction is a research area currently studied by Pierik et al. [36].

2.5.2. Sliding velocity
The sliding velocity has a large influence on the friction response considering the visco-elastic nature of the matrix material, and it has been investigated in several studies [5, 18, 19, 21, 31].

Extensive research on the influence of sliding velocity on the shear stress response has been conducted by Pierik et al. [20, 21, 31]. The influence of velocity seems to be similar in ply-ply and tool-ply friction. It was found that the peak during start-up became more dominant for relatively high velocities. In the most extreme case, the peak friction response quadrupled the steady state response. The peak disappears for relatively low velocities where the shear stress gradually increased until reaching a steady state. Another finding is that there is no increase in the steady state response for a sliding velocity ranging from 25 to 125 mm/min. It looks like the steady state response reaches an asymptotic value with increasing sliding velocity. This suggests that above a certain critical velocity, the velocity has little to no influence on the shear stress in the steady state region.

So, the sliding velocity appears to have a greater influence on the peak behavior rather than the steady state behavior. This suggests that the peak and steady state responses are caused by two different mechanisms. Or at least, a different combination of mechanisms. Pierik et al. [20], explained this by attributing the peak shear stress to a purely viscous shear flow of a matrix interlayer between two adjacent plies. The steady state shear stress would be caused by a severe reduction of this shear stress due to the onset of strong wall slip at the fiber-matrix interface.

2.5.3. Fiber orientation
There are countless different combinations of fiber orientations possible when designing a composite part. It is unavoidable that different combinations of fiber orientations are found between adjacent plies in a single part. In this section, the influence of different layups on the friction response of UD composite plies will be discussed.

Ply-ply effect
Several studies have been found where the ply-ply friction response with varying layups has been investigated [15, 18, 30]. A clear observation is that the peak response of plies consisting of fibers aligned with the sliding direction is higher than for plies where one of the two has a different orientation [18]. This effect would become more severe with increasing temperature, because the commingling of fibers is easier with the higher viscosity of the matrix material. Dörr et al. [15] observed an increase in peak behavior for an orientation of (90°/0°/90°) compared to (0°/0°/0°) as well. For relatively high sliding velocities, also a decrease in steady state response was observed for (90°/0°/90°) layups compared to plies with aligned fiber orientations. This has been explained by the commingling of fibers from the different plies during pre-consolidation when the fiber orientation of two adjacent plies is the same [18]. Another explanation given in the literature is that a clear inter-facial layer of matrix material cannot form during the consolidation of two plies with the same fiber orientation and therefore intra-ply shearing would take place before inter-ply slippage [30]. The actual explanation for the behavior could be a combination of these two theories.

Tool-ply effect
Tool-ply friction shows similarities to ply-ply friction regarding the influence of fiber orientation. Plies that have fibers in the same direction as the sliding direction offer more resistance against sliding than plies that have fibers in the direction orthogonal to the sliding direction [19]. Just a 10° deviation from the sliding direction already decreased the overall friction response [35].

2.5.4. Temperature
The temperature has a large influence throughout the entire hot press forming process. It has to be controlled precisely to produce defect-free parts. Besides crystallization, temperature also influences the viscosity of the matrix polymer melt and could affect how the sliding velocity influences the friction. The viscosity is in most studies captured in a rheological model. The temperature has a high influence on such models. A temperature increase of a shear thinning polymer melt leads to a reduction in viscosity for the same shearing rate [37].

Little research has been conducted in the field of temperature variation during friction characterization. In most cases, the minimum temperature has been set relatively close to the typical processing temperature. However, the tool temperature is much lower than this typical processing temperature. It is therefore likely that the laminate is colder than the typical processing temperature during the shaping of the laminate. In this subsection, the currently known effects of temperature on the friction response are discussed.

Two studies have been found where the effect of a temperature below the melting point on friction in woven composites was investigated [8, 17]. It was shown that lowering the temperature leads to an increase in both the peak and steady state friction response. The sliding velocity seems to have a more dominant effect on the friction response at lower temperatures (still above the melting point), resulting in higher peak overshoots during start-up [17]. When the temperature is lowered severely below the melting point, a new phenomenon is noticed. Instead of a peak in force followed by a steady state, the required load starts oscillating after reaching a certain threshold value. This is illustrated in Figure 2.13. The composite used in this research was a woven G/PP, PP has a melting point of around 160 °C. The oscillating effect is already visible at a temperature of 140 °C but becomes obvious at 135 °C.

This wobbling effect at low temperatures is caused by the woven character of the fabric used. From the data, it appeared that one cycle in the cyclic behavior at 135 °C corresponded to the same displacement as the width of a single roving in the fabric. The temperature reduction has increased the viscosity significantly, leading to a limited flow of matrix material and thus the rovings of the adjacent plies started passing over each other [17]. An important observation made during this research was that in the tests above the melting temperature, intra-ply shear also played a role. A high level of distorted fibers was visible when looking at a cross-section of a sample tested at a higher temperature. However, in the test specimens used in the test at 135 °C, a highly sheared layer of matrix material was visible and the fibers were not distorted. So it seems that the viscosity reaches a threshold value where inter-ply

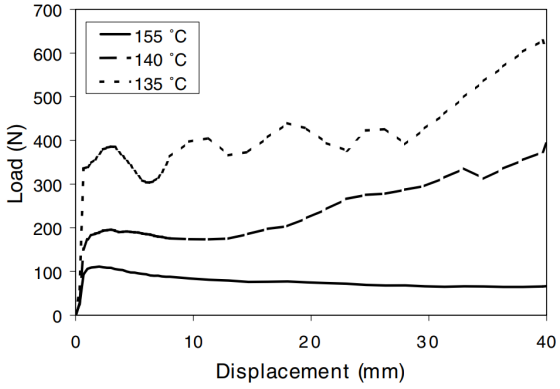

Figure 2.13: Results of a pull-out test with 2x2 glass fabric/PP composite in a ply-ply friction test setup, velocity of 20 mm/min. and normal pressure of 69 kPa [17].

slip becomes more dominant than intra-ply shearing [17]. This will be less obvious in UD composites because there is practically no intra-ply shear if the plies are pulled in the direction of their fibers [17].

The previously described test results were part of an investigation of a fabric-based composite. The cyclic load behavior at lower temperatures was a useful observation but given the explanation for this behavior, it is not expected to occur in UD composites. Murtagh and Mallon [35] have investigated the influence of temperature on the friction of UD composites but at a much higher temperature region. They reported that the steady state ply-ply shear stress response decreases with increasing temperature for a UD thermoplastic composite with a (90°/0°/90°) fiber orientation. However, as has been explained in Section 2.5.3, this influence might be different for other layups.

Only one study was found that focuses on the friction behavior below the melting temperature of the polymer in a UD composite [18]. The studied material is UD C/PEEK and the investigated temperatures are respectively 354, 343 (which is the melting point of PEEK) and 324 °C. The cyclic behavior at temperatures below the melting temperature was not found in this research, which substantiates the explanation for the behavior in woven fabrics. It was observed that the height of the peak in the friction response increased by a factor ten from 354 to 343 °C and again a factor four from 343 to 324 °C. The steady state response increased less as the temperature was lowered. A factor two increase was seen when lowering the temperature from 354 °C to 343 °C. The steady state friction response remained constant when lowering the temperature from 343 °C to 324 °C. It was also found that at a temperature of 324 °C, the fiber orientation of the plies did not influence the friction response anymore, whereas it did have an influence at higher temperatures. This observation led to the conclusion that when matrix material flow is limited, the friction is not influenced by fiber orientations. Considering that only three different temperatures are used in the research by Morris and Sun [18], and only one of these temperatures is below the melting point, more expanded research would have to be conducted to characterize the friction below the melting point properly.

2.5.5. Temperature distribution during hot press forming

A composite laminate is build up from multiple plies, the total thickness is determined by the number of plies. One could argue that the temperature curve given in Figure 2.4 is not applicable on each ply. The central plies have a nearly uniform temperature after leaving the heating stage. The outer plies are approximately 15 °C warmer [38]. However, during transport to the hot press and the forming stage, the outer plies will be subjected to more severe cooling than the center plies. In this case, the temperature distribution in the through-thickness direction of the laminate will be dependent on the thermal conductivity of three media, the composite material, the air during transport and the tool material.

A test with thermocouples between the plies during hot press forming can be used to measure the temperature distribution in the through-thickness direction. Such a test has been conducted at TPRC

with a woven G/PA-6 [38]. The used laminate consists of eight plies and the melting point of PA-6 is around 220 °C. The tool temperature in this specific test has been 150 °C. From the results, it has been observed that the two outer ply-ply interfaces instantaneously cool down to the tool temperature once contact with the mold has been made. A maximum cooling rate of over 2000 °C/min. is achieved. The second interfaces cool down significantly slower. The remaining central interfaces cool down with a similar rate of approximately 460 °C/min. [38]. A decline in the temperature at the outer interfaces is visible after transport from the oven to the press is initiated. The other interfaces remain constant. However, the measured decline is only marginal and it can be assumed that the laminate has a uniform temperature when mold contact is initiated. The described test consists of a specific material with a specific geometry resulting in unique data. However, it does give an indication of the temperature distribution in the composite laminate. In other research at TPRC, where a single thermocouple was placed in a C/PEEK composite laminate, similar cooling rates in the order of 10^3 °C/min. were achieved.

The results of these tests are of interest when determining the temperature window for friction characterization experiments. Together with this, an appropriate cooling rate can be established for which the friction behavior should be studied further. It can be concluded that for the most realistic simulation of the real process, one has to conduct non-isothermal friction characterization tests. But this requires a highly advanced setup where a temperature profile can be used during a friction test.

2.5.6. Velocity and temperature combination

During hot press forming and experimental friction characterization, temperatures are typically high enough for the thermoplastic polymer to melt. When performing rheometry experiments with a polymer melt, temperature and time appear to be interchangeable. This phenomenon is referred to as the time-temperature-superposition (TTS) principle [39]. In the case of friction characterization experiments, when regarding the sliding velocity as a duration parameter, a similar effect may occur.

TTS is a well-known method where the assumption is made that temperature and time can be exchanged with each other. The method is based on the observation that when recording rheological data over time, at a specific temperature, the shape of the curve does not seem to change with temperature but only shifts in a particular direction [39]. Using TTS, multiple tests on different temperatures can lead to similar results as one extensive test at low temperatures. The widely acclaimed method is mostly used in studies investigating time-dependent rheological properties [40, 41].

The coupling between temperature and time is called the temperature shift factor. It is a factor rather than a term due to the logarithmic nature of rheological data. This factor can be described by a Williams-Landel-Ferry model [42] or the Arrhenius model [43]. One of these models can be fitted to experimentally obtained temperature shift factors. Using this fit, temperature shift factors can be predicted and thus material properties in a broader range can be obtained without time-intensive experiments.

2.6. Crystallization

Several factors influence the crystallization of a polymer. It can be expected that the presence of fibers enhances the complexity of the crystallization kinetics [44]. Also the cooling rate is of influence on the crystallization, it strongly affects the onset temperature [45]. The crystallization kinetics of a thermoplastic polymer can also be influenced by shear flow which complicates the problem.

Flow-induced crystallization (FIC) is crystallization that takes place due to an accelerated nucleation rate which is induced by lining up the polymer chains by shear flow deformation [46]. But also extensional deformation can accelerate the crystallization rate or increase the onset temperature of crystallization [47]. The shear flow or extension aligns the longest chains which decreases the amount of entropy in the system. This reduces the energy barrier for nucleation [48]. From earlier research, it appears that the impact of shear flow on the acceleration of crystallization can be directly measured by the specific work induced by the shear [46, 47, 48], see Equation 2.3.

$$W = \int_0^{t_s} \eta(\dot{\gamma}) \cdot \dot{\gamma}^2 \, \mathrm{d}t = \eta(\dot{\gamma}) \cdot \dot{\gamma}^2 \cdot t_s \tag{2.3}$$

Where W is the specific work in J/m^3, t_s is the total shearing time, γ is the shear rate and η is the viscosity at this shear rate. FIC has been investigated earlier for multiple thermoplastic polymers [46, 47, 48]. From Equation 2.3, it can be seen that even with relatively short shearing times, still a relatively high specific work can be achieved as long as the shearing rate is high. A thin polymer interlayer forms between two adjacent plies during hot press forming or friction characterization, which results in relatively high shear rates. It is therefore plausible that FIC can occur during friction characterization at temperatures below the melting point of the thermoplastic polymer. This does not necessarily have to harm the hot press forming process but it needs to be taken into account when assessing the friction response at lower temperatures during experimental characterization. No studies have been found where the influence of FIC on the hot press forming process or friction characterization has been investigated.

2.7. modeling friction behavior

To accurately and quickly predict the shaping behavior of a laminate during hot press forming, a faster tool is needed than conducting friction experiments every time. A simulation tool, predicting the forming behavior, is in this case much more useful. A model to predict the friction response can be used as input for such a simulation software. Throughout the literature, a specific friction model is in most cases combined with a viscosity model for the polymer melt. In this chapter, a description of several distinct models will be given to get an overview of the different ways to approach the problem. To get a perspective, the different models are described in chronological order of the date of publishing.

2.7.1. Tool-ply friction model based on Stribeck-curve theory

In 2007 Gorczyca-Cole et al. [8] compiled an empirical friction model based on the Stribeck curve theory. According to Stribeck, a COF can directly be related to the so-called Hersey number [49]. The Hersey number H is given in Equation 2.4 [8].

$$H = \frac{\eta \cdot V}{N} \tag{2.4}$$

η is here the viscosity of the lubrication media, the molten polymer, V is the sliding velocity and N is the normal load. In Equation 2.4, the temperature and shear rate are also of influence by the viscosity of the molten polymer. So it is possible to obtain the same Hersey number for a different temperature or sliding velocity, as long as the other parameters are altered accordingly. One can plot the COF versus the Hersey number and this is called the Stribeck curve [8]. Using an extensive range of experimental parameters, part of the Stribeck curve can be generated experimentally. Gorczyca-Cole et al. [8] proposed a method of data fitting and applying a temperature shift to be able to predict the COF with the obtained data.

In the publication of this model, it is not mentioned if the obtained COF represents the peak behavior during start-up or the steady state response [8]. In the functions that are fitted to the data, the pulling force is taken as a constant with respect to displacement. This leads to the assumption that the resulting COF of this model is the steady state friction response. This is important to take into account when applying the model. The method has been validated by Sachs [5]. He confirmed that it proved reliable for fabric-reinforced thermoplastics, but that the theory does not hold for composites with UD fibers. Another important note is that Gorczyca-Cole et al. [8] assumed a matrix interlayer thickness before being able to compute the shear rate and thus the viscosity of the polymer material. However, it is not proven that this thickness is constant throughout the process. Another disadvantage is that first a high number of friction characterization experiments has to be conducted before the method can be used. This has to be done for every new material.

2.7.2. Tool-ply friction model based on Reynolds equation

Ten Thije et al. used a unit cell approach to implement the geometry of a fabric weave into a model to predict friction in tool-ply slip [34]. This model utilizes the Reynolds equation for thin film lubrication [49], which is initially deduced from the Navier-Stokes equations [50]. Different from the Stribeck curve theory, the pressure inside the thin film is not assumed to be constant. It is included by calculating the pressure build-up in the thin film, induced by the geometry of sliding surfaces.

The Reynolds equation reduces to Equation 2.5 assuming no density changes, a steady state slip, no geometrical deformations and only flow of matrix material in the direction of the slip. For more details on this, the reader is referred to the original paper [34].

$$\frac{\partial}{\partial x}\left(\frac{h^3}{\eta}\cdot\frac{\partial p}{\partial x}\right) = 6U\frac{\partial h}{\partial x} \tag{2.5}$$

In Equation 2.5, the variable U is the relative velocity in the slipping direction (x), h is the thickness of the film, p is the pressure and η is the polymer viscosity.

The cross-section of a weave is elliptical when it is slipping across a flat tool. This means that the film thickness varies in the direction of sliding. The film thickness $h(x)$ can be expressed as h_0 + $h^*(x)$, where h_0 is a constant and $h^*(x)$ is based on the geometry of the weave. Pressure builds up during slipping due to the geometry, leading to a bearing force [49]. It also leads to the flow of the polymer leading to a viscous friction force. The boundary conditions of the pressure profile can be used to solve Equation 2.5 for x, where the pressure is zero. This x-value can be used to compute the critical bearing length L_c. However, a value for h_0 is needed for this and this value is unknown [34].

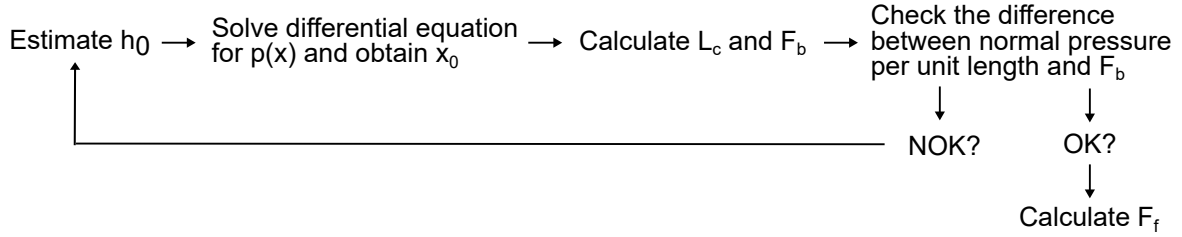

Figure 2.14: Flow chart of the iterative model to calculate the correct value for h_0 and apply this to calculate the frictional force per single weave.

The iterative model displayed in Figure 2.14 is used to calculate the bearing force (Equation 2.6) and equate this to the applied normal pressure using a specific value for h_0. These forces should be equal since the weave is not moving normal to the slipping direction. With the correct film thickness h_0 found, the total friction force per weave can be calculated according to Equation 2.7 [34].

$$F_\mathrm{b} = \int_{L_\mathrm{c}} p(x)\,\mathrm{d}x \tag{2.6}$$

$$F_\mathrm{f} = \int_{L_\mathrm{c}} \tau(x)\,\mathrm{d}x \tag{2.7}$$

If this iterative model is applied to every type of weave in a laminate and multiplied to obtain the specific dimensions of the laminate, a total friction force can be calculated.

For relatively low velocities, the model slightly overpredicts the actual COF. The model slightly underpredicts the COF for relatively high velocities. In general, a good fit is observed to the experimental results. But the model cannot be applied to UD composites as they do not exhibit such severe film thickness variations causing a pressure build-up [5]. Hence, Sachs [5] used a different approach to predict the UD tool-ply friction response in the model that is discussed next.

2.7.3. Mixed lubrication model for UD tool-ply friction

U. Sachs [5] used a different approach by splitting the total friction force into a dry contribution and a viscous contribution. This model assumes that after reaching a critical shear stress, wall slip between the fibers and the matrix interface layer decreases the friction. It is assumed that a laminate is incompressible in the thickness direction and that the applied normal force is transferred to the tooling by the fiber network. This results in dry contact points between the laminate and the tool where the fibers touch the tool surface. On the locations where the fibers do not touch the tool, viscous shearing of the polymeric matrix material will take place. With a set of assumptions, an estimation can be given of the total number of dry contact points per unit area [5].

The frictional force by the dry contact points is the total dry contact area times the interfacial shear strength. The size of an individual contact area can be determined with the Hertzian contact model [49], using the total normal load divided by the number of contact points per unit area.

The viscous friction force is deducted from the viscous shear stress in the matrix material and integrated over the remaining contact area (A^{visc}) after subtracting the dry contacts from the total area. The shear stress is dependent on the shear rate and the viscosity of the polymeric material at that specific rate and temperature. A 1D flow in the direction of slipping is assumed. After reaching a certain critical shear stress τ^{crit}, wall slip between matrix material and tooling is assumed and which leads to velocity increases without further enlargement of the shear stress. The work by Hatzikiriakos [51], who performed extensive studies on wall slip with pure polymers, proved valuable to estimate a critical shear stress τ^{crit}. This all leads to Equation 2.8 and Equation 2.9 for the viscous friction force [5].

$$\tau^{\text{visc}} = \text{min.}\left(\dot{\gamma} \cdot \eta(\dot{\gamma}, T), \tau^{\text{crit}}\right) \tag{2.8}$$

$$F_{\text{f}}^{\text{visc}} = \int \tau^{\text{visc}} \, \text{d}A^{\text{visc}} \tag{2.9}$$

The viscous and the dry contribution are simply added to calculate the total friction response. The prediction can be validated by a pull-out or pull-through test. Due to the dry contact friction, normal pressure is of high influence in this model. For relatively high normal pressures, the model prediction becomes more accurate. This is an indication that the inaccuracy could be lying in the dry contact contribution. Altogether, the model represents the experimental results only at high sliding velocities, but only if the matrix film thickness has been investigated microscopically and if the wall slip behavior and especially the onset of wall slip is measured rather than estimated [5].

2.7.4. UD ply-ply friction model based on wall slip

The 3 models described above are all compiled to model and predict tool-ply friction. Only one effort, by Pierik et al. [20], has been found where the ply-ply friction response of UD composites is modeled.

In the model by Pierik et al. [20], the friction response is separated into the typical peak and the steady state response. The model assumes a simple one-dimensional shear flow that causes the peak. When the matrix material starts slipping along the fibers, the response evolves into a steady state. This occurs after a critical shear stress has been achieved like in the model by U. Sachs in Section 2.7.3. The main difference lies in the fact that this is a ply-ply friction prediction rather than tool-ply friction. Also, the surface roughness of the fibers themselves have not been taken into account in this model and a matrix material interface layer between the two plies is assumed. In the currently discussed model, the critical shear stress is obtained through experiments rather than an assumption as is the case in the model by Sachs [5].

To calculate the simple shear flow in this model, the thickness of the matrix interlayer between two plies is needed. This can be obtained from cutting used specimens and observing the cross sections in an optical microscope. However, an easier way is to use randomly generated fiber distributions to obtain an artificial matrix interlayer thickness. This method proved itself as a reliable one according to the published results [20].

If two adjacent plies move with a relative velocity V, then the matrix material that forms the interface layer will be sheared with a local shear rate $\dot{\gamma}$. This shear rate is then given by Equation 2.10 when assuming 1D flow.

$$\dot{\gamma} = \frac{V}{h(x)} \tag{2.10}$$

Here $h(x)$ is the height of the interface layer and the x-axis lays in the direction of the width of the ply and at the exact center of a generated fiber distribution [20]. To obtain the shear stress, a rheological viscosity model has to be used. In the research where this model is established [20], UD C/PEEK was used and the Cross model was the best fit to the viscosity data, see Equation 2.11 [37].

$$\eta(\dot{\gamma}) = \frac{\eta_0}{1 + (\frac{\eta_0 \cdot \dot{\gamma}}{\tau^*})^{(1-n)}} \tag{2.11}$$

Here, η_0 is the zero shear-viscosity, $\tau^\star$ is critical shear stress and n is the Power Law index. The reciprocal of $\frac{\eta_0}{\tau^\star}$ is an indicator of the onset shear rate of the shear thinning region. The local shear stress τ^{visc} is the product of the local viscosity and the local shear rate as given in Equation 2.12. But the thickness of the matrix interlayer $h(x)$ is not constant. Therefore an average shear stress is computed across the total width of the matrix interlayer w, see Equation 2.13.

$$\tau(x) = \eta(\dot{\gamma}(x)) \cdot \dot{\gamma}(x) = \eta\left(\frac{V}{h(x)}\right) \cdot \frac{V}{h(x)} \tag{2.12}$$

$$\tau_{\text{avg}} = \frac{1}{w} \int_0^w \tau(x)\ \mathrm{d}x \tag{2.13}$$

If one assumes a critical shear stress τ^{crit} for the onset of wall slip, then the local shear stress becomes the minimum of either the viscous shear stress or this critical shear stress [51]:

$$\tau(x) = \text{min.}\left(\eta\left(\frac{V}{h(x)}\right) \cdot \frac{V}{h(x)}, \tau^{\text{crit}}\right) \tag{2.14}$$

So with a larger shear rate, the viscosity-induced shear stress increases while the critical shear stress remains constant. Because it is a local shear stress, one by one, local shear stresses will achieve this critical shear stress and strong wall slip will become dominant [51]. Following this, the friction response will reach the steady state of strong wall slip [20]. In order to obtain the actual average shear stress, Equation 2.13 and Equation 2.14 are to be combined.

The film thickness $h(x)$, is the crux of this model. It is time-consuming to cut specimens every time and to prepare the cross sections for optical microscopy. Along with that, it can be rather difficult to distinguish the actual slip interface in these micrographs [20]. Therefore, an attempt has been made with a randomly generated fiber distribution across a baseline, to mimic the ply-ply interface. The fiber distributions are generated with the algorithm by Melro et al. [52]. It appears that this method yields just as accurate results compared with real micrographs of specimen cross-sections. This has to do with the fact that the fibers are in general homogeneously distributed in an actual micrograph, making the location of a slip interface arbitrary [20].

A series of pull-through tests are conducted and compared to the model to validate the accuracy. These tests also provide one with a critical shear stress. From the tests, it appeared that after reaching a certain sliding velocity, the steady state response reached an asymptotic value and did not increase further. This plateau steady state shear stress can be utilized as critical shear stress for the onset of strong wall slip as it does not seem possible for the shear stress to achieve a higher value in the steady state [20]. The model is accurately predicting both peak and steady state responses by implementing a critical shear stress. For more details on the comparison between the model and the experimental results is referred to the original paper [20].

For this model, the Cross viscosity model was used, and the tests were conducted at the same temperature [37]. But it is yet unknown what will happen if the temperature is altered. The viscosity will likely shift, causing the critical shear stress to be achieved earlier for lower temperatures and later for higher temperatures. This is only from a viscosity point of view, if the temperature also influences the interlayer thickness then the mechanism would become more complex, and perhaps the model would not represent the experimental data properly anymore. Further investigation in the lower temperature range is needed to verify the model for other temperatures than the typical processing temperature.

2.8. Literature gap

An introduction to the topic has been given in Chapter 1 and an outline of the corresponding literature has been discussed in the current chapter. With this, it is possible to identify the gap in literature that requires further research and is thus the main motive for the research conducted in this thesis.

Three different gaps in the literature can be identified:

- Knowledge about the friction behavior in UD thermoplastic composites, at significantly lower temperatures than the processing temperature, is still lacking. Research has been conducted on this field [18], but an expansion in experimental parameters is needed to appropriately formulate any conclusions about the friction behavior at such a low temperature.
- Temperature not only affects the thermoplastic material in terms of rheology but also crystallization can start to play a role at relatively low temperatures. To aid in understanding the causes for forming issues due to increased friction, it is of interest to look into the thermoplastic polymer at lower temperatures. This information can be used to explain any changes in the friction behavior compared to the behavior at higher temperatures.
- Predictive models proposed in Section 2.7 [5, 8, 20, 34] have been benchmarked against experimental data at typical processing temperatures for the used material. It is yet unknown how accurate these models are at significantly lower temperatures. Using experimental data, a comparison and validation can be conducted in a larger temperature range.

3

Experimental method

The used methodology to characterize the ply-ply friction response will be presented in this chapter. Along with this, an explanation of the used setup will be given. The thermo-analytical experiments with composite material will be outlined along with the used parameters. Rheological experiments have been used for two different purposes, the specifics and goals of both experiments will be given. At last, the methodology of the FIC experiment will be given.

3.1. Materials

The same composite material has been used throughout the research. Samples have been cut from larger rolls of Toray Cetex TC1225 [53]. This is a thermoplastic composite material consisting of semi-crystalline Victrex LM-PAEK AE250 strengthened by carbon fibers. The fibers are UD oriented in the tangential direction of the supplied rolls. The matrix material has a melting temperature of 305 °C and a typical processing temperature of 340 to 385 °C, according to the manufacturer. The supplied rolls of composite material are approximately 30 cm (12 inch) wide. The outer 5 cm of the rolls are discarded and not used in any experiment since a stronger influence of the production process can be expected here compared to the center. This reduces the possibility of experimental result scattering by non-homogeneity of samples.

3.2. Thermal analysis

Differential scanning calorimetry has been used to obtain the thermal properties of the composite material utilizing a TA DSC 250. Also, the neat polymer matrix material has been analyzed to establish any influences by the fibers on the thermal properties. The neat polymer matrix material (in powder form) has been supplied by the manufacturer of the composite, Toray Advanced Composites.

Smaller pieces that fit the sample pans of the DSC have been cut from the rolls of composite material. Each sample weighs between 4 and 7 µg. Sample pans provided by TA Instruments have been used along with the corresponding encapsulation press. An empty reference pan is used to calibrate the measurements. Samples are loaded by a built-in auto-sampler.

3.2.1. Thermal properties

To validate the thermal properties presented by the supplier of the composite material, several DSC tests have been performed. Both with the LM-PAEK powder and with the carbon fiber reinforced LM-PAEK to examine the influence of the fibers on the thermal properties. With both materials, five different tests have been conducted consisting of two thermal cycles. The first cycle is used to obtain information about the glass transition temperature, melting temperature and potential re-crystallization. The second cycle is performed to investigate the influence of the cooling rate on the crystallization temperature without any influence from the initial production process. The investigated cooling rates are 7, 25, 35, 45 and 60 °C/min. The temperature profiles are given in Table 3.1.

Table 3.1: Temperature profiles of DSC analysis to obtain thermal properties of both the neat matrix material (LM-PAEK) and the composite material (C/LM-PAEK). *Rate X is either 7, 25, 35, 45, 60 °C/min.

Action	Duration	Rate
Equilibration at 40 °C	-	-
Heat to 365 °C	-	20 °C/min.
Isotherm at 365 °C	5 min.	-
Cool to 50 °C	-	7 °C/min.
Isotherm at 50 °C	5 min.	-
Heat to 365 °C	-	20 °C/min.
Cool to 50 °C	-	X* °C/min.

3.2.2. Representation of temperature during friction characterization

The temperature profile used to obtain a specific heat flux versus temperature curve has to be prescribed. The profiles used in this experiment are a representation of the sample temperature during a friction test and they are presented in Table 3.2. The cycle is repeated once after completion, to investigate the influence of the thermal history on the material. The isothermal step of 6 minutes is corresponding to the dwell and measurement time during an actual friction characterization test. The results from the thermal analysis can be used to determine whether crystallization occurs during friction characterization tests.

Table 3.2: Temperature profiles of DSC analysis to investigate isothermal crystallization. *Temperature X is either 365, 345, 330, 315, 300 or 270 °C.

Action	Duration	Rate
Equilibration at 40 °C	-	-
Heat to 365 °C	-	20 °C/min.
Isotherm at 365 °C	5 min.	-
Cool to X* °C	-	7 °C/min.
Isotherm at X*	6 min.	-
Cool to 40 °C	-	20 °C/min.
Repeat process	-	-

3.3. Rheometry experiments

An Anton Paar Physica MCR 501 rheometer has been used to obtain the rheological properties of the neat matrix material. This is a plate-plate rheometer, both plates are 25 mm in diameter. A mechanical hot press is used to produce disc samples from the polymer powder. The powder is placed in a disc-shaped mold with a diameter of 25 mm and a thickness of 1 mm. The press is heated to 340 °C and a force of 40 kN is used to press the mold together. The disc sample is placed between the two plates of the rheometer and heated to 365 °C. The excess material is trimmed away after reaching the correct temperature and positioning the plates in the measuring position with a 0.8 mm gap width.

First, an oscillatory amplitude sweep with a constant radial shear rate of 1 rad/s is performed. The resulting storage and loss moduli versus radial shear strain is used to determine the linear visco-elastic domain of the material. 1% Radial shear strain is approximately in the middle of this domain and is thus used in a series of frequency sweeps.

Oscillatory frequency sweeps between 0.1 and 500 rad/s and a strain amplitude of 1% have been conducted to obtain the complex viscosity as a function of angular frequency. The temperature for the frequency sweeps has been 365, 345, 330, 315 and 300 °C. Each measurement has been conducted

three times and the results are averaged. The resulting complex viscosity versus angular frequency curves are converted to viscosity as a function of shear rate by applying the Cox-Merz rule [54]. Continuous shearing tests have been performed at relatively low rates to validate the Cox-Merz rule. The obtained viscosity data is fitted with the Cross model given in Equation 2.11 [37].

3.4. Ply-ply friction characterization

A Zwick friction tester has been used for the characterization of the ply-ply friction response. This specific friction tester has been benchmarked in earlier research by Sachs [5]. For this setup, a specific sample has to be prepared. It consists of one composite ply in the middle (I in Figure 3.1b) with a shorter ply (IV) on both sides of it. The sample dimensions are given in Figure 3.1c. The fibers are oriented in the longitudinal direction. The composite plies have a middle section of 5x5 cm^2 where they overlap, the friction is characterized here. The alignment and positioning of the composite plies relative to each other are standardized for every measurement with a 3D-printed alignment tool. The normal stress and temperature of the overlap are controlled by two heated clamping blocks (II in Figure 3.1b). These blocks are shielded from melting matrix material by disposable steel foils (III). The inner and outer surfaces of the plies in the sample have a specific orientation with respect to the originally supplied material roll. This orientation has been kept constant throughout the research. In addition, the top and base of each ply have been kept constant with respect to the rolling direction. The two shorter composite plies are fixed by a stationary clamp at the bottom. The middle ply is clamped at the top, this clamp moves with a constant rate in the vertical direction during the experiment. The alignment of the sample to the direction of motion is confirmed with a self-leveling laser light.

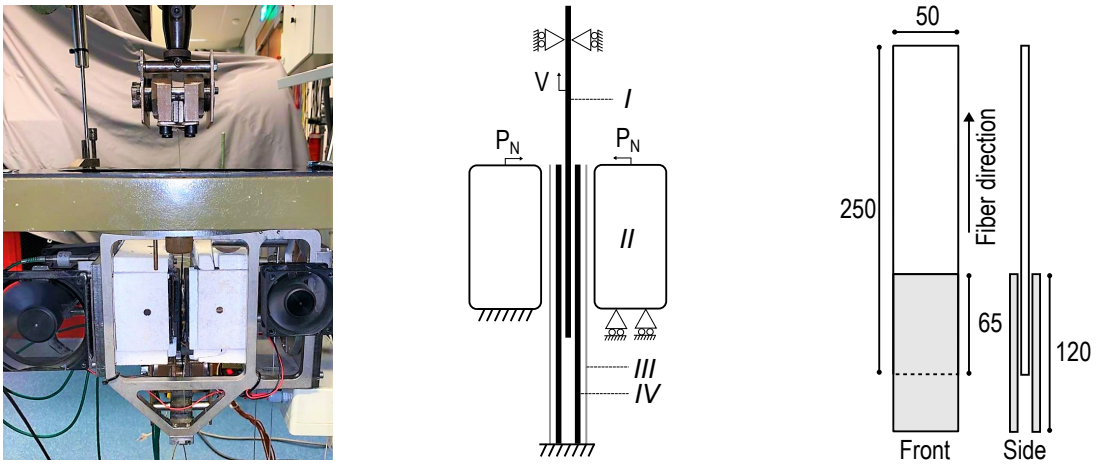

(a) Camera shot of Zwick friction tester.

(b) Zwick friction tester. I: moving ply, II: heat block, III: steel foil, IV: stationary composite ply.

(c) Sample and dimensions in mm, all plies have a thickness of 0.14 mm.

Figure 3.1: The Zwick friction tester along with an outline of the samples and their dimensions.

The required load, to pull the middle ply from between the other plies and heating blocks, is logged during an experiment. Using the known slip surface area, the shear stress can be computed from this load according to Equation 3.1. The required load is denoted by F in N and the slipping surface is denoted by A in m^2. The middle ply slips on both sides, therefore the surface is multiplied by 2.

$$\tau = \frac{F}{2 \cdot A} \tag{3.1}$$

The sliding velocity of the ply is controlled by the setup. The heat blocks have a length of 50 mm (surface area of 25 cm^2) but the overlap of the plies is 65 mm in length, see Figure 3.1c. The additional overlap is used to be able to slip at least 10 mm with 5 mm as a safety margin. The sample is heated to 365 °C and then cooled to the desired characterization temperature with a rate of 7 °C/min. It is first heated to 365 °C, to fully melt the thermoplastic material and obtain a uniform temperature. It would be desired to have a higher cooling rate to achieve the characterization temperature, but this is not

possible in the used setup. A 5-minute dwell time at the characterization temperature has been used to obtain thermal homogeneity and to prevent inconsistencies between measurements regarding dwell time. The duration of a single experiment can be calculated beforehand by using the prescribed sliding velocity and slip distance of 10 mm. The motion is stopped manually after this specific amount of time. The data logging continues after standstill to obtain relaxation and residual stress data. Hereafter, the load required to lift the upper clamp and sample is logged to correct for the gravity.

The friction has been characterized at 5 different velocities of 10, 25, 40, 75 and 125 mm/min. The temperature has been varied between 300, 315, 330, 345 and 365 °C. The normal pressure has been kept at 15 kPa for every measurement. A complete overview of the experimental parameters is given in Table B.1 of Appendix B.

3.5. Flow-induced crystallization

As was explained in Section 2.6, FIC may occur during friction characterization at relatively low temperatures. To investigate the severity of FIC at the lowest characterization temperature of 300 °C, a set of experiments has been conducted.

A DSC-experiment has been used to validate that during 6 hours at 300 °C, no crystallization occurs in the LM-PAEK powder when the sample is not subjected to shear flow deformation. An Anton Paar Physica MCR 501 rheometer with 25 mm parallel plates has been used for the main FIC experiment. Discs are pressed from neat polymer powder as has been explained in Section 3.3. These discs are made from the same polymer as the matrix material in the composite plies that have been tested during friction characterization. After placing the discs between the parallel plates in the rheometer, they are heated to 365 °C before starting the FIC experiment. After an isothermal period of 5 minutes at 365 °C, the temperature is reduced to 300 °C with a rate of 10 °C/min., while preventing an undershoot after 300 °C has been reached. Immediately after reaching 300 °C, the sample disc is sheared with a constant rate for a duration of 250 s. Following the period of constant shear, an oscillatory time sweep is performed with a relatively low strain amplitude of 0.5% and angular frequency of 5 rad/s. The storage and loss modulus are logged during this time sweep. The phase shift angle δ can be determined from these moduli using Equation 3.2.

$$\tan(\delta) = \frac{G''}{G'} \tag{3.2}$$

In Equation 3.2, G'' is the loss modulus and G' is the storage modulus. The loss modulus represents the viscous behavior of a polymer melt, whereas the storage modulus represents the elastic behavior. If crystallization starts in the polymer melt, the ratio of the viscous and elastic behavior will change in favor of the elastic contribution. This means that due to crystallization, δ will decrease. This way, the duration for the phase shift angle to reach a value of 50° can be used as an indicator of the crystallization time [48]. If FIC does indeed occur, then an increasing constant shear rate during the period before the time sweep should decrease the crystallization time. Or in this case, the time before the phase shift angle has reached a value of 50°.

Different constant shear rates have been tested, ranging from 0 to 70 s^{-1}. A new sample and new rheometer plates have been used for every experiment. The furnace of the rheology meter is constantly flushed with nitrogen gas to prevent degradation of the polymer during the measurements. After each experiment, the sample is heated to 365 °C again and a frequency sweep is performed. This is also done before the experiment has started. The results of the frequency sweep before and after the FIC experiment are compared to confirm that the polymer has not undergone any other changes during the FIC experiment.

4

Modeling

When designing a hot press forming part, it can be beneficial to predict the forming behavior by use of simulations. To do this, one first has to be able to predict the friction behavior as this is one of the main deformation mechanisms. Different approaches can lead to a different prediction of the friction behavior with varying accuracy. In this research, three different approaches will be compared to the obtained experimental data from the friction characterization. The methods are explained in this chapter, along with their similarities and differences.

Each of the three discussed approaches assumes that an interlayer consisting of matrix material forms between two plies in a ply-ply friction test. Using the varying height of this matrix interlayer in the transversal direction and the prescribed velocity of the friction test, a corresponding shear rate of the matrix material can be calculated. Using the viscosity of the matrix material obtained according to the method described in Section 3.3, one can calculate a local shear stress depending on the local shear rate. Taking the average of these local shear stresses gives a single value for the viscous shear stress response. Assuming no wall slip occurs during the peak behavior of the shear stress response of a friction test, this viscous shear stress should correspond to the value of the peak [20]. Introducing a critical shear stress for the onset of wall slip results in a local maximum shear stress. This influences the total average viscous shear stress and can be used as a prediction for the steady state shear stress response in a ply-ply friction test. This method, to predict both the peak and steady state behavior is explained in more detail in Section 2.7.4 [20]. The difference between the three approaches is the way the geometry of the matrix interlayer is determined. The three different ways of composing a matrix interlayer are the algorithm by Melro et al. [52], the Darts algorithm composed in this research, at last, an equivalent film thickness is used.

4.1. Algorithm by Melro

The first approach is the one used by Pierik et al. as described in Section 2.7.4. A generated fiber distribution from the algorithm by Melro et al. [52] is used to obtain the geometry of a matrix interlayer. This interlayer is used to predict the peak and steady state behavior during a friction test as described above. The algorithm uses 50.000 attempts of randomly placing non-overlapping fibers in a rectangle. However, a relatively high fiber volume fraction (59%) cannot be achieved by this method alone. Therefore the fibers are stirred in the next step, obtaining a higher local fiber density in specific locations and thus providing space for extra fibers. This is a highly dynamic step where almost every fiber is translated slightly in a single iteration, at the same time new fibers are placed in the new free space. For more details on this process is referred to the original research paper [52].

After the fiber distribution has been generated, the interface of two plies is assumed to be in the center of a single fiber distribution. The interlayer thickness is assumed to be the transversal distance in the through-thickness direction between the fibers that are closest to this specific line. An example of a resulting matrix interlayer is given in Figure 4.1.

Figure 4.1: Fiber distribution obtained with the algorithm by Melro et al. [52] along with matrix interlayer (vertical distance between solid lines), deduced with central interface line (dashed line).

4.2. Darts algorithm

In the second approach, developed for this research, two rectangles are pseudo-randomly filled with circles of prescribed radius until a specific ratio of the total surface is filled with circles. The algorithm is called the Darts algorithm. The rectangle corresponds to the outlines of a cross-section of a UD composite ply, the circles represent the fibers and the area ratio is the fiber volume fraction. For each newly placed fiber, a test is conducted to confirm that it does not overlap with fibers placed earlier. Using this method it is rather difficult to obtain large fiber volume fractions because they are not placed in a more optimal location to enhance local fiber density. Therefore, after reaching a fiber volume fraction of 0.8 times the desired fiber volume fraction a new mechanism is activated. After every 5000 failed iterations the algorithm removes a fiber from the total set. Failure is in this case defined as when a newly generated fiber overlaps with one or more earlier-generated fibers. The fiber that is being removed is the one that is the furthest away from its closest neighbors but is still within a distance of less than a fiber diameter from these closest neighbors. The flow chart of the darts algorithm is schematically displayed in Figure A.6 of Appendix A.

The two generated fiber distributions are then placed on top of each other and translated toward each other until they intersect. The top outline of the lower fiber distribution is then subtracted from the bottom outline of the upper fiber distribution to calculate a matrix interlayer thickness. Examples of generated fiber distributions along with the matrix interlayer thickness are given in Figure 4.2. To remove the effects from the sides of the fiber distributions, only the central 80% of the width of the matrix interlayer is used for further calculations.

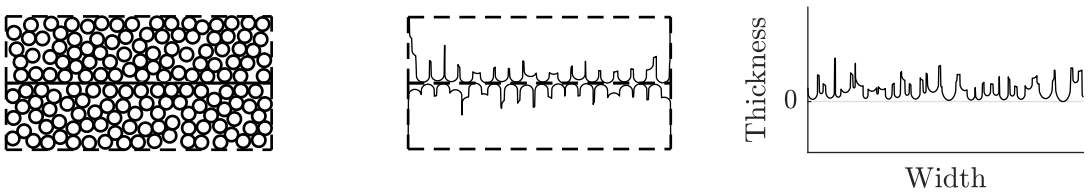

(a) Two separately generated fiber distributions placed on top of each other.

(b) Outlines of both generated fiber distributions outlined along the interface.

(c) Total interlayer thickness neglecting the outer ends of the fiber distributions.

Figure 4.2: Generated fiber distributions and calculated matrix interlayer thickness. All three images are scaled to each other.

Calculating a viscous shear stress to resemble the peak shear stress in a friction test is done in the same way as in the first approach by Pierik et al. [20]. Also, the steady state response is predicted in the same way. The main difference between the two methods is the way the fiber distributions are generated. This leads to a geometry for the matrix interlayer that is characteristic of the used method.

4.3. Equivalent film thickness

In the third and final approach, the problem is simplified. The matrix interlayer is assumed to be a film with uniform film thickness. This equivalent film thickness can then be used to calculate the viscous shear stress to predict the peak response. When a critical shear stress is imposed for the onset of

wall slip, a distinct transition will be visible from viscous flow to wall slip because the shear stress is uniform in the transversal direction. Consequently, this means that the prediction of the steady state shear stress is equal for every sliding velocity once peak behavior is visible.

5

Results

The results from the experimental work and the different modeling approaches will be discussed in this chapter. First, the results from the thermal analysis, the viscosity curves and the results from the FIC experiments will be presented, along with the raw results from the friction characterization. In the second part of this chapter, a further analysis of the friction characterization will be given. The experimental data will be compared to the modeling efforts.

5.1. Thermal analysis

Using DSC, several thermal properties of both the C/LM-PAEK composite and the neat polymer material have been obtained. First, the glass transition temperature, re-crystallization temperature and melting range of the composite material have been determined during heating from room temperature to 380 °C, see Figure 5.1. Next, the sample is cooled to room temperature again with a relatively low rate of 7 °C/min. The same parameters have been determined in a second cycle to exclude any influence by the original production process. The re-crystallization peak disappears in the second cycle and the glass transition fades away. The melting peak narrows during the second cycle compared to the first one and the melting peak temperature shifts two degrees upwards.

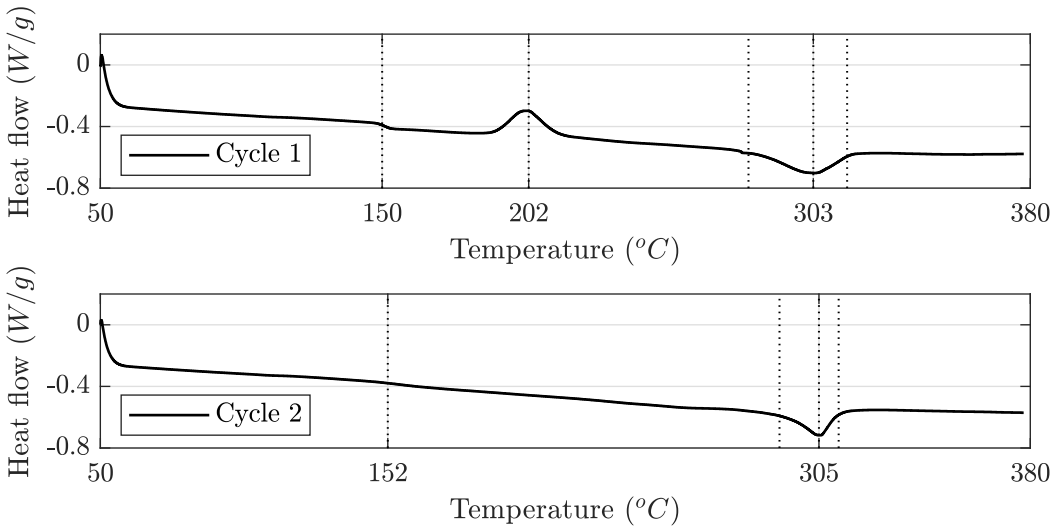

Figure 5.1: Heating of C/LM-PAEK with 20 °C/min. during DSC. Relevant temperatures are indicated. The onset of melting is 280 °C and the endset is 315 °C during cycle 1. The onset of melting is 291 °C and the endset is 312 during cycle 2. Y-axis represents exothermic flow.

The onset of crystallization with varying cooling rates has been measured for both the composite material and the neat matrix material, aiming to investigate whether the presence of fibers influences

the onset of crystallization. The results are given in Figure 5.2. It can be seen that the surface below the peaks is larger for the pure powder specimens (Figure 5.2a) compared to the C/LM-PAEK (Figure 5.2b). The most striking observation from this experiment is the shift in the onset of crystallization. Apparently the fibers are influencing the onset temperature. Where the onset temperature for a rate of 7, 25 and 60 °C/min. is 274, 261 and 251 °C, in the LM-PAEK powder, it is 258, 244 and 233 °C in the C/LM-PAEK composite.

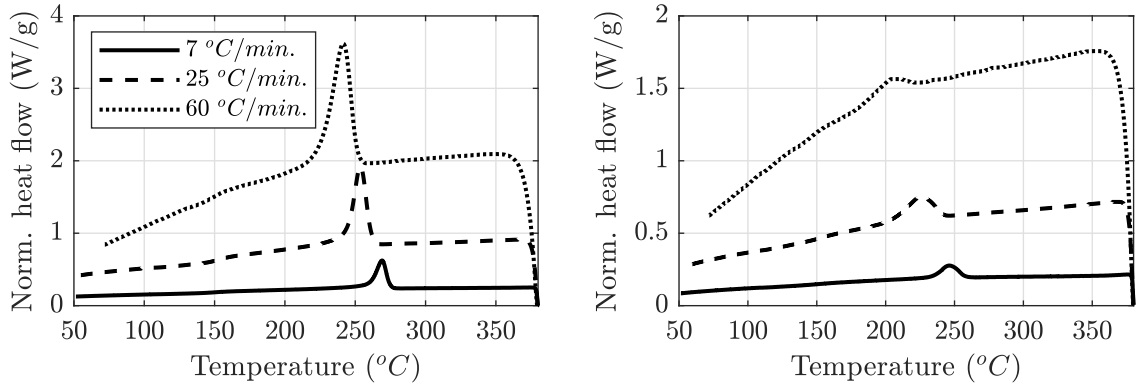

(a) LM-PAEK powder.

(b) Carbon fiber reinforced LM-PAEK.

Figure 5.2: DSC curves during cooling with different rates of both neat and carbon fiber reinforced LM-PAEK samples. Cooling started after an isothermal period of 5 min. at 380 °C. The legend applies to both graphs and the Y-axis represents exothermic flow.

DSC also has been used as a method to investigate the influence of crystallization during friction characterization. The temperature profile during the friction test has been mirrored during a DSC test. See Section 3.2 for more details on the build-up of the specific temperature profiles. The heat flow and temperature over time for two of these tests can be seen in Figure 5.3 and Figure 5.4. In the figures is the normalized exothermic flow versus time displayed.

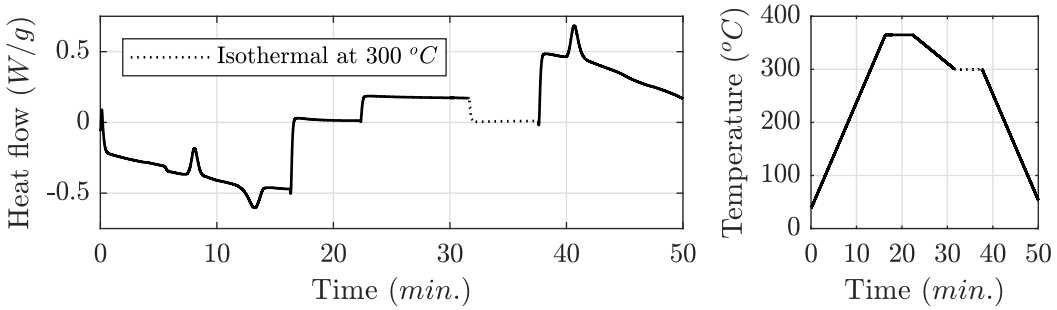

Figure 5.3: DSC curve of carbon fiber reinforced LM-PAEK together with used temperature profile corresponding to a friction characterization test at 300 °C. Y-axis represents exothermic flow.

In Figure 5.3, a clear exothermic peak representing crystallization can be distinguished after the isothermal period at 300 °C. In Figure 5.4, the onset for crystallization is before or during the isothermal period at 255 °C. These two different DSC tests are part of a broader range of DSC experiments to investigate the influence of crystallization during experimental friction characterization. The results of the tests with an isothermal period at 365, 330 and 270 °C can be found in Appendix A. The highest temperature, where crystallization is seen during the isothermal period, is 270 °C.

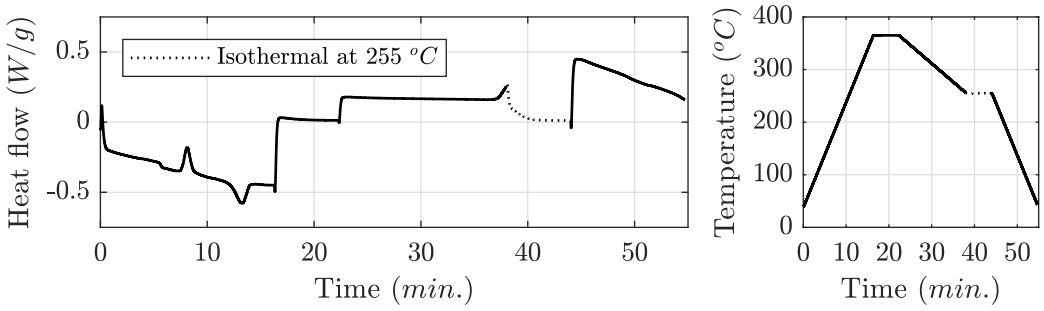

Figure 5.4: DSC curve of carbon fiber reinforced LM-PAEK together with used temperature profile corresponding to a friction characterization test at 255 °C. Y-axis represents exothermic flow.

5.2. Rheometry

The measured viscosity curves of the neat matrix material for different temperatures are shown in Figure 5.5. The data has been fitted to the Cross model given in Equation 2.11, which shows to be an appropriate fit for the obtained data. The curves and the data points, which are averages from experiments in triplicate, are displayed in Figure 5.5 along with error bars corresponding to a 95% confidence interval. The same neat polymer material has been investigated in a study by Pierik et al. [20]. The viscosity curve at 365 °C presented in their work corresponds to the curve in Figure 5.5.

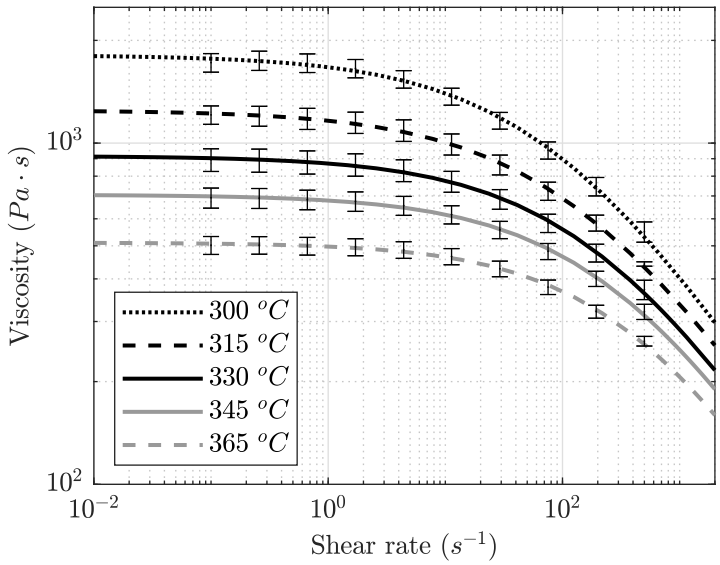

Figure 5.5: Viscosity curves obtained with experimental rheological data fitted to Cross model. The error bars represent the 95% confidence interval of 1.96 times the standard deviation in both positive and negative directions. Cross model fitted parameters are for 300 °C: $\eta_0 = 1811.4$ Pa · s, $\tau^\star = 176363.0$ Pa, $n = 0.462$. For 315 °C: $\eta_0 = 1247.8$ Pa · s, $\tau^\star = 186819.8$ Pa, $n = 0.476$. For 330 °C: $\eta_0 = 916.6$ Pa · s, $\tau^\star = 210621.2$ Pa, $n = 0.456$. For 345 °C: $\eta_0 = 705.8$ Pa · s, $\tau^\star = 233579.4$ Pa, $n = 0.445$. For 365 °C: $\eta_0 = 510.9$ Pa · s, $\tau^\star = 261221.1$ Pa, $n = 0.421$.

Validation of the Cox-Merz rule, as was stated in Section 3.3, has been conducted at 365 °C for relatively low shear rates. The resulting viscosity shows an overlap with the complex viscosity results from the oscillatory frequency sweeps. This overlap lasts up to a shear rate of 10 s^{-1}, the data starts to diverge hereafter. The data from both experiments are displayed in a single figure in Figure A.1.

A frequency sweep with 1% strain amplitude was performed at 365 °C with a gap height of 0.9, 0.8 and 0.7 mm. This has been done to validate the gap height between the parallel plates during the

rheometry measurements and to rule out any influence on the results. The pressed LM-PAEK sample discs have a thickness of approximately 0.95 mm. From the experiment, it appears that a gap height of 0.9 mm still gives deviating results but reducing the gap height to 0.7 or 0.8 mm gives two exactly similar curves. The results of the test are displayed in Figure A.2 for more details.

5.3. Friction characterization

A series of friction characterization experiments has been conducted, aiming to characterize the friction response at temperatures lower than the typical processing temperature. The exact input parameters of every experiment can be found in Table B.1. The results presented in this section are averages of three experiments with identical parameters. The average result from every set of parameters is presented in Figure 5.6. In this section, the friction characterization results are presented along with a few general observations. A detailed analysis of the results from the friction characterization will be given in Section 5.5, along with a comparison to the models discussed in Chapter 4.

The friction characterization results can be displayed in different ways. In Figure 5.6, the results from each set of experimental parameters are displayed in shear stress versus slip distance graphs. In general, a higher sliding velocity results in an increase in peak height of a typical friction response, the peak also becomes sharper. For a relatively low sliding velocity, the opposite occurs as the peak reduces in height, increases in width and sometimes even disappears. These two observations regarding the friction curve were also discussed in Section 2.5.2. However, the changes in the peak behavior were there caused by an altered sliding velocity and a constant temperature. In the current research also the temperature is varied, which apparently leads to a similar effect. When changing both parameters at the same time, this effect is even greater.

When maintaining sliding velocity and reducing the temperature, a plateau value for the steady state shear stress is visible in Figure 5.6. Where the peak shear stress severely increases, the steady state shear stress barely changes.

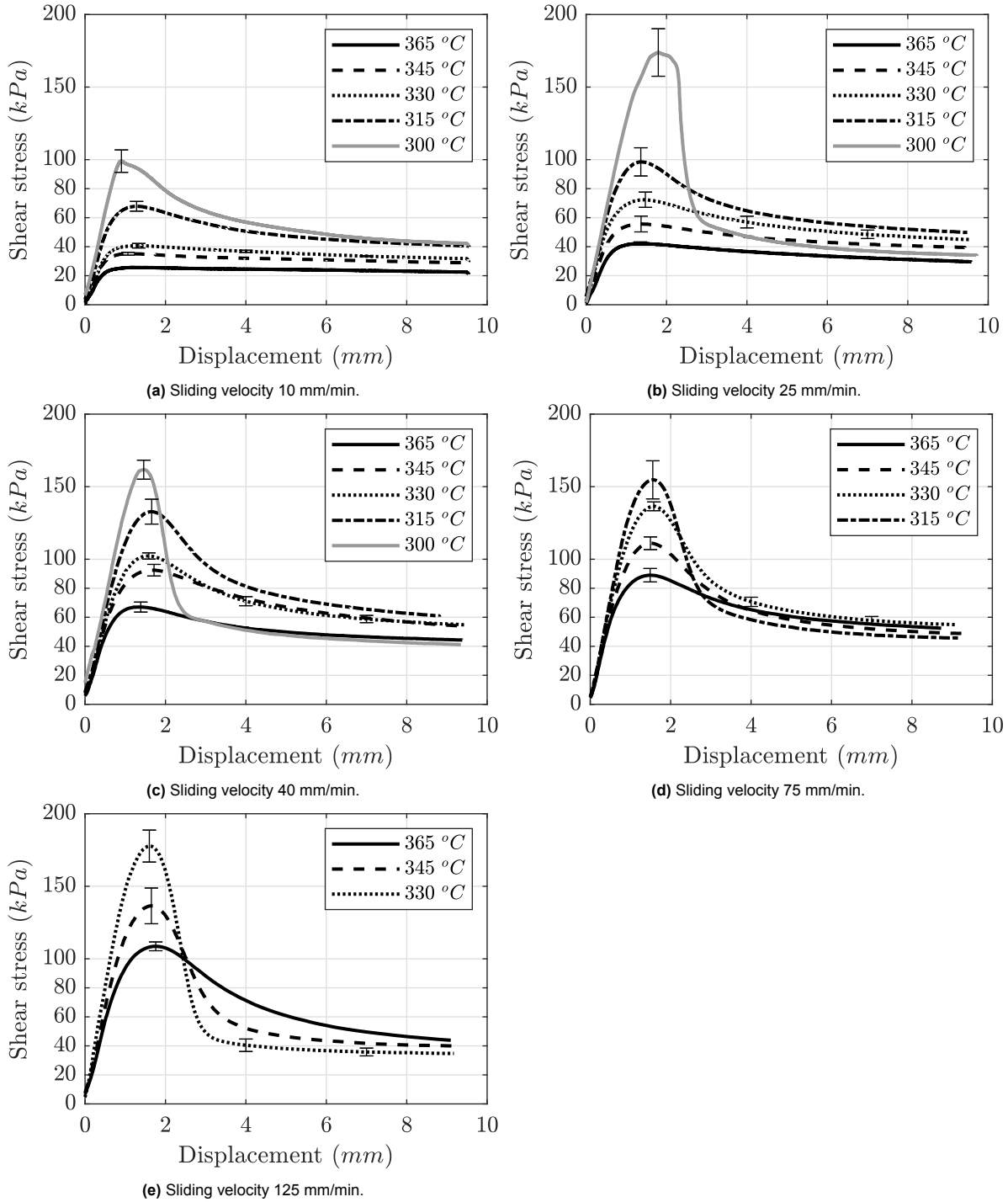

(a) Sliding velocity 10 mm/min.

(b) Sliding velocity 25 mm/min.

(c) Sliding velocity 40 mm/min.

(d) Sliding velocity 75 mm/min.

(e) Sliding velocity 125 mm/min.

Figure 5.6: Results from ply-ply friction characterization with varying sliding velocity and temperature. Fiber orientation is kept constant with an orientation of (0°/0°/0°), and the normal pressure has been kept constant at 15 kPa. Each curve is an average of three separate measurements with different samples. Error bars represent the standard deviation of the three measurements at the peak along with 4 and 7 mm of slipping distance in the curve at 330 °C.

5.4. Flow-induced crystallization

A significantly higher residual stress is measured after stopping the friction characterization measurement at 300 and 315 °C (for more details, see Figure A.7). This effect is the largest for a sliding velocity of 10 mm/min. at a temperature of 300 °C. Clear stress relaxation is visible for higher temperatures where the stress approaches zero after the friction measurement has been stopped. This was not the case for lower temperatures where a residual stress remained.

The results from the FIC experiments described in Section 3.5 are given in Figure 5.7. The most striking observation is that the baseline measurement, where the sample has not been sheared with a constant rate before the oscillatory time sweep, also shows a significant increase in storage modulus after a certain time period. For the samples that are sheared, the phase shift angle does indeed decrease more quickly. However, this effect does not grow with a higher shear rate. For a shear rate of 70 s^{-1}, no significant difference with the baseline measurement is seen.

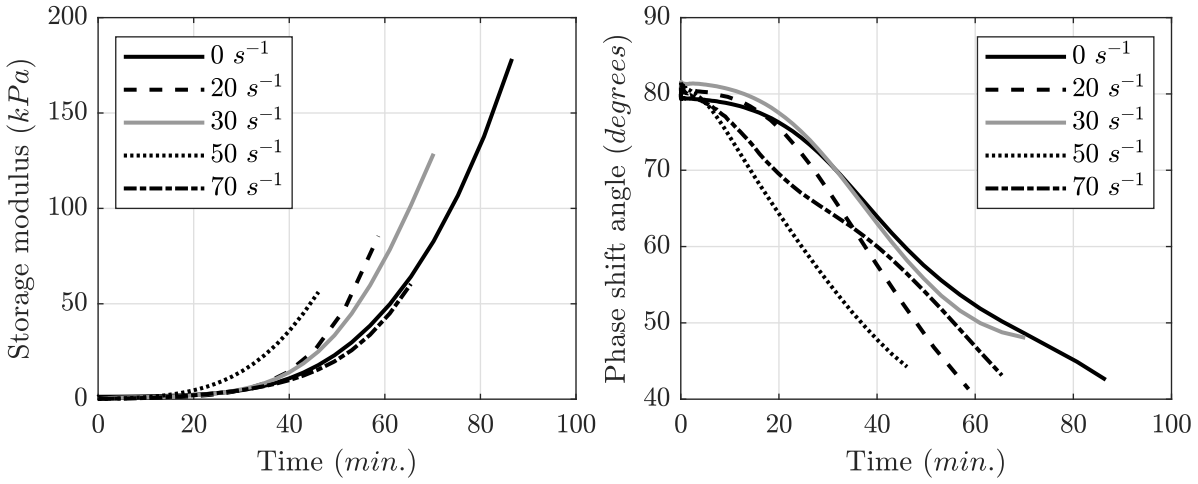

(a) Storage modulus versus time.

(b) Phase shift angle versus time.

Figure 5.7: The oscillatory time sweep at 300 °C, with strain amplitude of 0.5% and angular frequency of 5 rad/s, after the samples have been subjected to a different shear rate for a duration of 250 s.

5.5. Friction characterization analysis

As stated before, a more detailed analysis of the friction characterization results will be given in this section. A straightforward approach is by identifying each friction curve into a peak response and a steady state response. The first one can be retrieved from the data by taking the maximum shear stress value. The latter one has to be determined by using a prescribed condition since a fully horizontal curve is not always achieved after a slipping distance of 10 mm. Therefore, a function of the form displayed in Equation 5.1 has been fitted to the data between 3.5 and 9 mm of slipping distance. This function has been chosen based on the fact that the mean squared error is relatively low and that exponential behaviour is physically possible in this specific situation. The point where a steady state has been achieved is set to be at the point where the derivative of this function fit is equal to -0.5 kPa/mm.

$$f(x) = a \cdot x^b + c \tag{5.1}$$

Because this method is a form of extrapolation, its accuracy has to be validated. Therefore it has been tested for the curves where a clear horizontal part is already visible in Figure 5.6. The same function fit is applied on these curves but now only with the data between 3.5 and 5 mm. This fit is extrapolated and the shear stress at the point where the slope is equal to -0.5 kPa/mm is compared to this same point in the actual curve. For the tested curves, this leads to an error in the extrapolation method of 2%.

With the peak and steady state shear stress quantified for each sliding velocity and temperature, the data can be displayed in a single plot such as in Figure 5.8.

In Figure 5.8 one can see the peak and steady state shear stress from every friction curve displayed as a point in a graph. For the peak shear stress, a gradual increase with sliding velocity is visible for

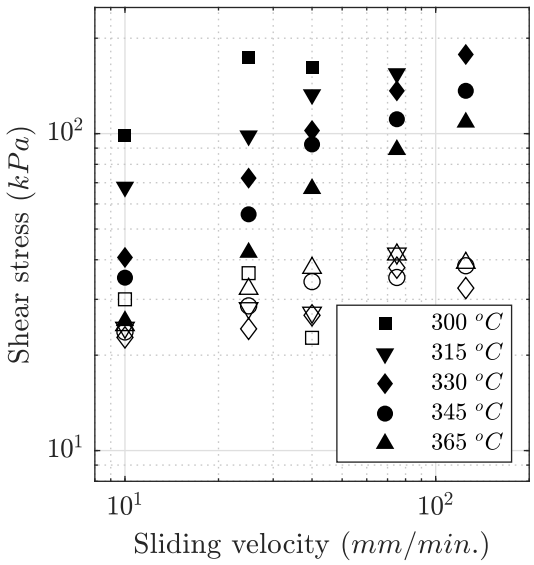

Figure 5.8: Peak and steady state shear stress response for each of the friction characterization experiments displayed on a logarithmic scale. The filled symbols represent the peak response and the open symbols represent the steady state response.

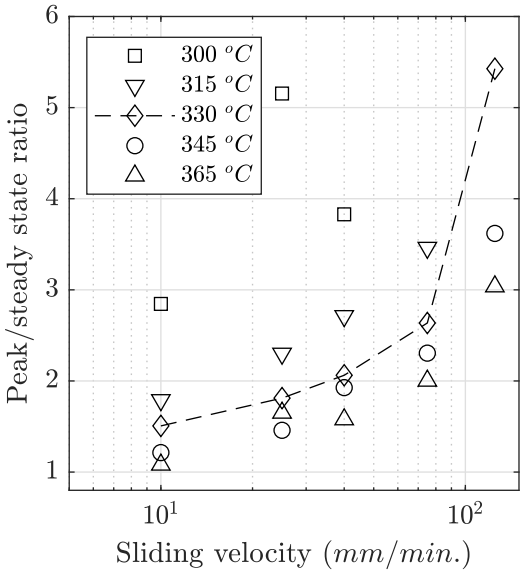

Figure 5.9: Ratio of peak shear stress response versus steady state with varying velocity and temperature. To aid the reader in distinguishing the overall trend, the scatter points at 330 °C are connected by a dashed line.

every temperature. The deviating behavior at 300 °C is more pronounced in the complete graphs in Figure 5.6. It can be seen here, that the peaks are rather bumpy even though it is an average of three measurements. Besides this, the friction curve at 300 °C and 25 mm/min. has a relatively high error.

There are two important observation from Figure 5.8. The first one is that the peak and steady state responses are similar at low sliding velocities and high temperatures. But with increasing sliding velocity they diverge, the onset of this divergence is earlier for lower temperatures. This is further emphasized in Figure 5.9. With this graph is shown that the minimum required sliding velocity to obtain significant peak behavior reduces for lower temperatures. To aid in distinguishing this trend, one of the data sets has also been displayed using a dashed line. The ratio appears to increase with increasing sliding velocity but also with decreasing temperature, suggesting an inverse relationship between temperature and sliding velocity. The second important observation in Figure 5.8, is the almost linear increase of the peak with sliding velocity where the curve seems to shift upwards with each temperature.

Another phenomenon is visible from the curves in Figure 5.6. It appears that the transition from peak to steady state is a faster process for lower temperatures with the same sliding velocity. This effect is even more clear when the shear stress is plotted against time as is displayed in Figure A.7. For curves at high temperatures, the transition is smooth, gradual and slow. When reducing temperature, this process is accelerated while at the same time the peak increases in height, e.g. the peak becomes sharper.

Measuring the average slope of the curve during the transition makes it possible to quantify the speed of the peak-to-steady-state transition. The difference in shear stress between the peak and the point, where the second derivative is at a maximum, is taken. This difference is divided by the time between the peak and this so-called turning point. This calculation can also be regarded as a calculation of the average drop of the curve in this specific section. When plotting the average drop versus sliding velocity and temperature, the influence of these two parameters becomes clearer, see Figure 5.10.

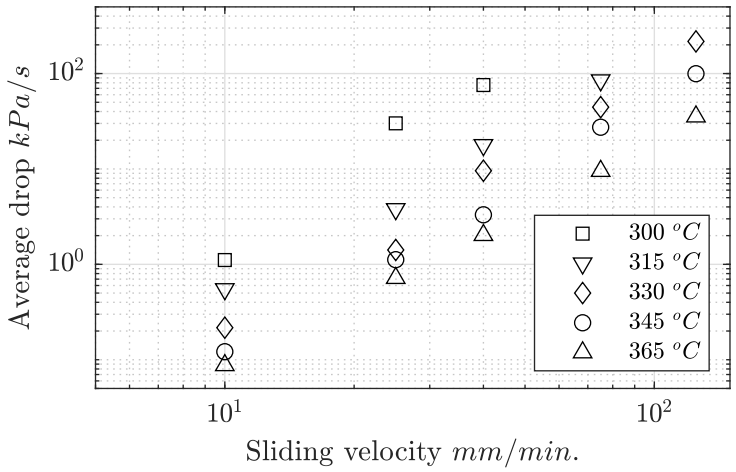

Figure 5.10: Average drop from peak up until turning point. Representing the speed of the transition from the peak towards steady state behavior.

All the scatter points for each temperature are located on a line. So, on a logarithmic scale, a simple linear function can be fitted to the data. The fits are displayed in Figure 5.11, and a shift with decreasing temperature is visible. This behavior has a high resemblance with rheological data of thermoplastic polymers. If the sliding velocity is regarded as a duration parameter, TTS can be applied to the data to generate a master curve at a reference temperature.

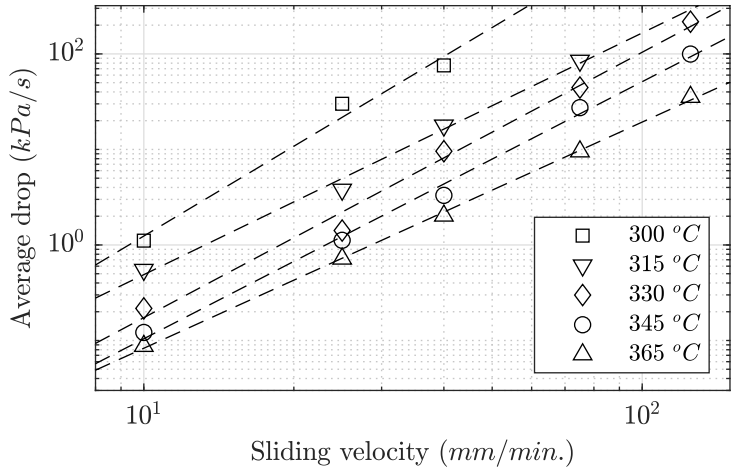

Figure 5.11: Average drop in the friction curves between peak and turning point along with fitted lines. R^2 of fits are 0.98, 0.99, 0.99, 0.995 and 0.999 for the temperatures 300, 315, 330, 345 and 365 °C.

Sections of the lines displayed in Figure 5.11 are shifted to generate a master curve at a reference temperature of 345 °C. The obtained master curve is displayed in Figure 5.12a. The shift factor (a_T) used for each temperature to obtain the master curve is plotted in Figure 5.12b along with an Arrhenius fit to the five data points, see Equation 5.2 [37, 39].

$$a_T = \exp\left(\frac{E}{R} \cdot \left(\frac{1}{T} - \frac{1}{T_{ref}}\right)\right) \tag{5.2}$$

$$\log_{10}(a_T) = \frac{E}{2.303 \cdot R} \cdot \left(\frac{1}{T} - \frac{1}{T_{ref}}\right) \tag{5.3}$$

R represents the universal gas constant and E is a fitting parameter representing the activation energy. The fit appears to overlap with most of the data points, but the measurements at 300 °C seem to deviate from the trend. The TTS principle to generate a master curve makes it possible to predict the average drop of curves at temperatures for which no measurements have been conducted yet. The value of this will be further explained in Chapter 6.

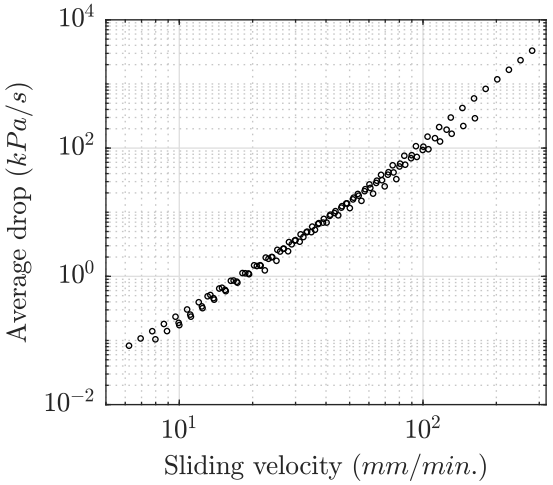

(a) Average drop master curve at the reference temperature of 345 °C.

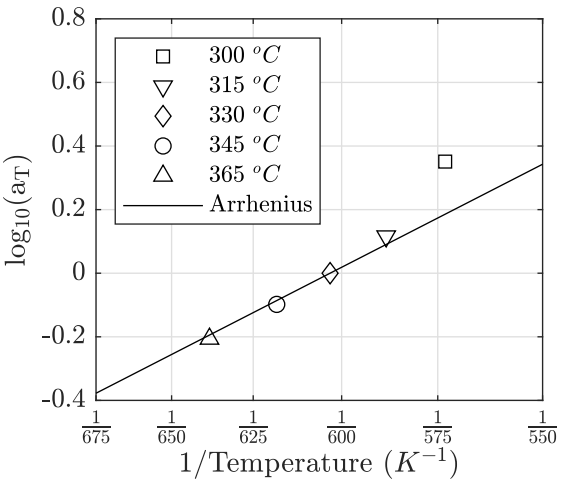

(b) Shift factor a_T used to construct the master curve depicted in Figure 5.12a. Plotted with Arrhenius fit with fit parameter E being 40.9 kJ. R^2 of Arrhenius fit is 0.845.

Figure 5.12: Mastercurve at a reference temperature of 345 °C along with the corresponding shift factor for each temperature.

5.6. Model comparison

As was discussed in Chapter 4, three different approaches to predict the peak and steady state shear stress response have been compared. The results of this comparison to experimental data will be presented in this section.

In Figure 5.13, the results from the prediction by using an equivalent matrix interlayer thickness at the ply-ply interface of 2.5 µm are displayed. A thickness of 2.5 µm has been obtained by means of trial and error to obtain the best fit for the experimental results. An equivalent matrix interlayer thickness of 2.5 µm also has been used in other research [21]. There are no error bars displayed since the prediction is not an average of multiple interlayer distributions but only one simple uniform matrix interlayer thickness has been used. Even though this is a blunt simplification of the problem, the peak shear stress is still predicted quite accurately. This accuracy reduces for higher sliding velocities which is also visible in the other models. The most important note is the section where the steady state prediction suddenly reaches the plateau value of 55 kPa which is the critical shear stress for the onset of wall slip in the model.

A more accurate prediction is achieved with the model used by Pierik et al. [20] where the algorithm by Melro et al. [52] is utilized to generate fiber distributions. The results from this model for both 330 and 365 °C are displayed in Figure 5.14. Error bars are displayed which represent the 95% confidence interval of 1.96 times the standard deviation in both positive and negative directions. This error originates from the fact that 10 different fiber distributions are used to obtain the average shear stress for each sliding velocity. The results for the temperatures 300, 315 and 345 can be found in Figure A.8.

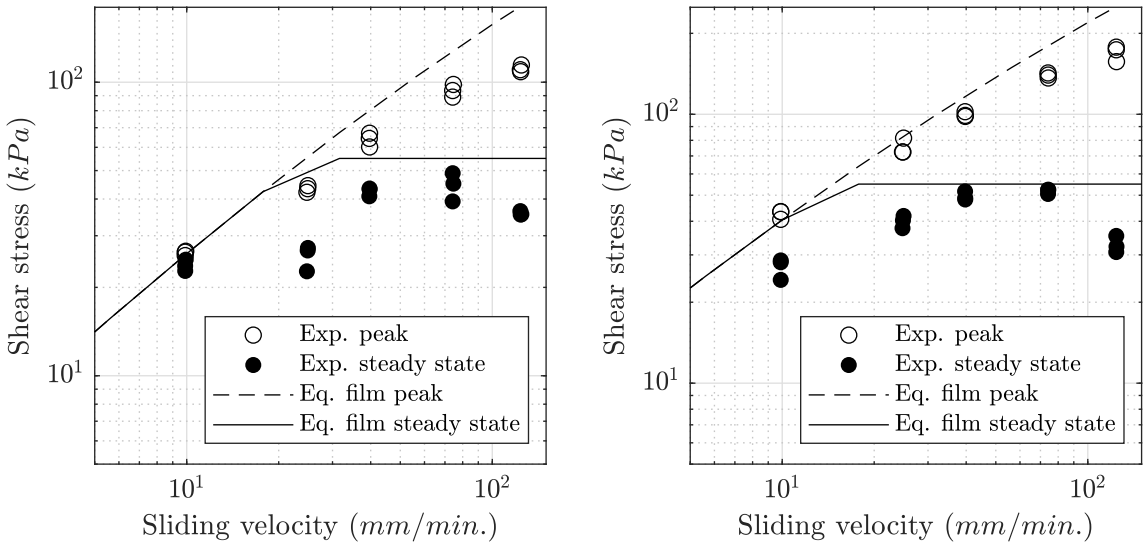

(a) 365 °C. **(b)** 330 °C.

Figure 5.13: Results from the prediction of peak and steady state shear stress by using an equivalent film thickness of 2.5 µm at both 365 and 330 °C.

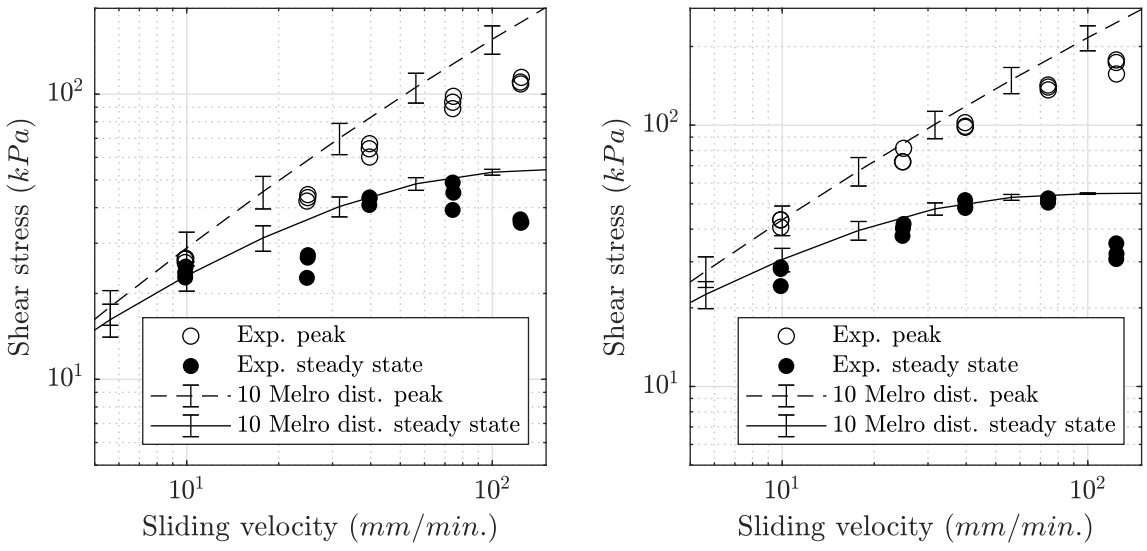

(a) 365 °C. **(b)** 330 °C.

Figure 5.14: Results from the prediction of peak and steady state shear stress at both 365 and 330 °C by using 10 fiber distributions generated with the algorithm by Melro et al. [52].

The model results displayed in Figure 5.14 appear to be closer to the experimental data at both temperatures. As the model is composed and tested at typical processing temperatures by Pierik et al. [20], it is striking that it still yields a high accuracy at 330 °C. A slight overprediction is visible for relatively high sliding velocities.

The results from the Darts algorithm, developed in this research, are displayed in Figure 5.15. The results for the temperatures 300, 315 and 345 °C can be found in Figure A.9. Similar accuracy can be seen compared to the results from the model by Pierik et al. [20]. However, one important difference in the results from the Darts model is that even for very low sliding velocities, the peak shear stress prediction is still significantly higher than the steady state stress prediction. In fact, the curve for the

predicted peak shear stress and the curve for the predicted steady state shear stress appear to become parallel for relatively low sliding velocities.

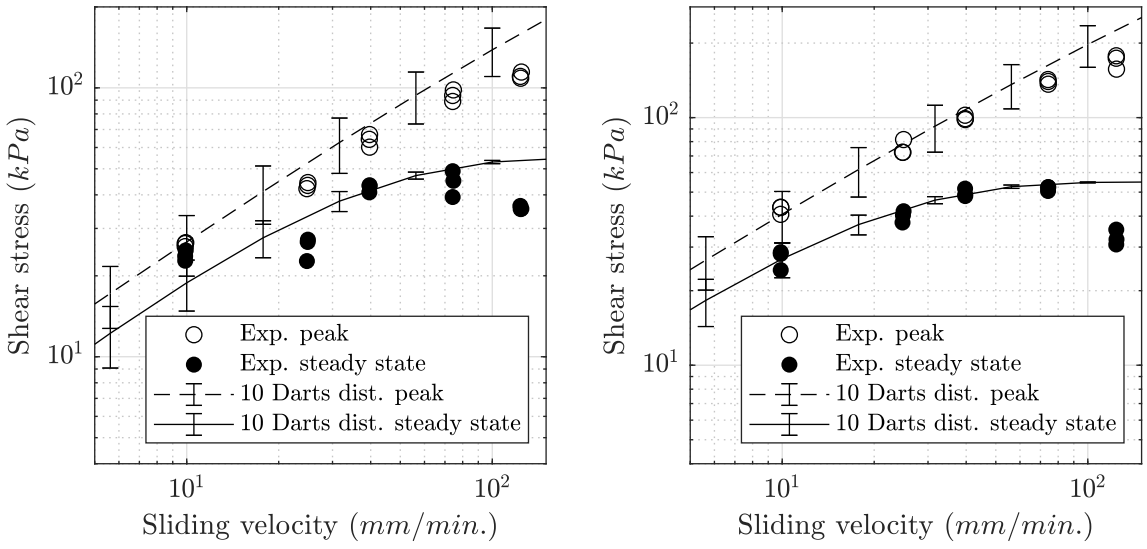

(a) 365 °C. **(b)** 330 °C.

Figure 5.15: Results from the prediction of peak and steady state shear stress at both 365 and 330 °C by using 10 fiber distributions generated with the Darts algorithm.

6

Discussion

The goal of this study has been to obtain a better understanding of the friction behavior of UD fiber-reinforced thermoplastics, with a specific focus on the influence of temperature. In this chapter, the gained insights will be emphasized and their value will be discussed. Besides this, also the boundary conditions and the general robustness of the research will be analyzed.

6.1. Value and impact

The value of the research will be outlined in this section. It will be explained per subject how this research can contribute to obtaining a better understanding of the friction behavior of UD fiber-reinforced thermoplastics. The most important conclusions originating from these findings are listed in Chapter 7.

6.1.1. Thermal analysis

In this research, DSC has been used to obtain the thermal properties of the used materials. Two different temperature cycles are presented in Figure 5.1. In the second cycle, the glass transition and re-crystallization peak have disappeared, this means that the thermal history is successfully erased during the first cycle. From the results of the cooling experiments given in Figure 5.2, it can be seen that pure polymer powder samples release more energy during cooling. This is visible by the enlargement of the surface below the crystallization peaks, which indicates a larger crystallization enthalpy. This phenomenon can be explained by the fibers (59% in volume) in the composite samples which are not experiencing any transition. A lower onset temperature for crystallization in the C/LM-PAEK compared to the neat LM-PAEK, regardless of the cooling rate, is also visible in Figure 5.2. So, besides the regular shift in crystallization onset temperature when varying a cooling rate [45], the fibers have a negative effect on the crystallization nucleation which results in a lower crystallization onset temperature.

From Figure 5.3 and Figure 5.4, it becomes clear that a certain amount of under-cooling is necessary for crystallization to play a role during a friction characterization experiment (dotted part of the DSC curve). When assuming no shear flow of the matrix material, and using a cooling rate corresponding to the used friction characterization setup, crystallization should not interfere with friction characterization experiments at 300 °C and higher. This can be concluded from the fact that in these DSC tests, the onset of crystallization has been after the isothermal period. But it must be emphasized that the DSC results are fully stationary and there is no shear flow in these samples at all.

The findings explained in this subsection are important when one is looking into the active mechanisms during friction characterization experiments. This information is valuable in excluding the possibility of isothermal crystallization during the experiments. Even though shear flow deformation of the matrix material is experienced during friction characterization, it is important to confirm that crystallization has not started already before the measurement.

6.1.2. Rheometry

The results from the experiment to validate the Cox-Merz rule can be found in Figure A.1. As indicated in Section 5.2, the data is diverging for shear rates higher than 10 s^{-1}. This can be caused by slight axial misalignment of the shafts in the used setup or by increased normal stress during testing. However, most likely is a change in sample geometry near the outer edges of the parallel plates [55]. The diverging effect is also seen in other studies. Nazari et al. [56] attributed this effect to the start of FIC in a viscosity test with PEEK. They stated that a shear rate with an order of magnitude 10 s^{-1} is high enough to obtain FIC. This effect can influence the obtained viscosity during a steady state frequency sweep. However, they performed the frequency sweep at a temperature closer to the melting point of the material compared to the current experiment.

From the validation of the gap height between the two parallel plates during rheological testing (Figure A.2), it has become clear that results are univocal with a gap height below 0.9 mm. This is the desired effect and it confirms that a standard gap height of 0.8 mm, as is used in this research, is an appropriate choice. The deviation at 0.9 mm may be caused by wall slip between one or two of the aluminum parallel plates and the polymer sample during the measurement [57]. Another explanation is a nonuniform distribution of polymer melt when the plates are 0.9 mm apart since the original pressed discs are only 0.95 mm in thickness.

Using both of these experimental validations and comparing the obtained results to the data provided by the manufacturer, Toray Advanced Composites [27], it can be concluded that the results are reliable. The value of these results lies in the fact that the viscosity can be used for further steps in the research. An example of this is using the viscosity data as input for the models given in Chapter 4.

6.1.3. Friction characterization

The goal of the experimental friction characterization has been to gain an understanding of the behavior at lower temperatures. The results given in Figure 5.6 provide more insight with friction curves for multiple sliding velocities at five different temperatures. At the same time, the scattering in the results at 300 °C is relatively high, which downgrades the value for the results at 300 °C. In this research, the increase in scattering at lower temperatures has always been seen together with increased residual stress after the measurement. It was therefore attributed to FIC, however, the behavior may have more than a single cause. The value and knowledge obtained by this is that friction characterization is not as straightforward at temperatures around the melting point, compared to temperatures at a typical processing temperature. Different mechanisms become active at lower temperatures, which means that the used setup is no longer measuring the same phenomena throughout the entire temperature range. This finding is something to take into account when designing new experimental plans or a new friction characterization setup.

One of the observations made in Section 5.3 is the plateau achieved for the steady state shear stress when reducing temperature while maintaining the sliding velocity. The same effect can be seen when increasing the sliding velocity but maintaining the temperature. A similar effect is observed in the literature [21]. In the specific study, the temperature has been higher but the results from the current research can confirm the behavior for relatively low temperatures.

Peak towards steady state transition

A relation with respect to velocity and temperature has been found for the average slope during the peak-to-steady-state transition in the friction curves. This relation is explained in detail in Section 5.5. The fact that the transition is faster for lower temperatures can be explained by the chain mobility of the polymer and wall slip. Wall slip is initiated after locally achieving the critical shear stress for the onset of wall slip [51]. This leads to a stationary boundary layer of polymer chains attached to the wall, while the polymer chains in the bulk are moving past this layer [51]. At higher temperatures, the polymer chains are generally more mobile and flexible [37, 39]. This leads to re-entanglement of the boundary layer and bulk polymer chains until the entangled chains are again fully relaxed and wall slip is initiated again. This causes a local stick-slip situation [51]. This is in line with the time-temperature-superposition principle. For higher temperatures, the chains are mobile enough to conform and adhere to the boundary layer and while doing so, increase the time of the peak-to-steady-state transition. For low temperatures

the chains are rather stiff and less mobile, preventing the re-entanglement with the bulk. This leads to a transition from viscous peak shear stress to the steady state wall slip that is much more abrupt as the polymer dynamics are inadequate to accommodate for the applied rapid shear deformation.

With the model by Pierik et al. [20], the height of the peak and the steady state shear stress response can be predicted accurately up to a certain sliding velocity. Also with the Darts algorithm, to generate fiber distributions, along with the method by Pierik et al., an accurate prediction of the peak and steady state response can be achieved. This knowledge can be combined with the ability to obtain an average slope during the peak-to-steady-state transition using the TTS principle (Figure 5.12a and Figure 5.12b). Using the peak shear stress, the steady state shear stress and the average slope, one can predict the time it takes to transition from the peak to the steady state. This can be of great value in forming simulation software. Not only a specific COF could be used for the peak and steady state behavior, besides this, a transition time dependent on temperature and sliding velocity can be used as an input parameter. After this duration, or transition time, the switch between peak and steady state friction should be made. This leads to a more dynamic and realistic approach to predicting the friction between plies during forming, which can lead to a higher predictive quality of the forming simulations.

6.1.4. Flow-induced crystallization during friction characterization

An important observation in the friction characterization results is the residual stress after the measurement. In the research by Pierik et al. [20, 21, 31], this residual stress has been subtracted from the peak and steady state friction response. This stress was attributed to the nature of the composite material in combination with the test method. It is assumed to be constant throughout testing and it would be caused by dry fiber contacts in the matrix polymer melt. This has been validated by Murtagh et al. [58].

However, in the current research is decided not to subtract this residual stress from the peak and steady state response. This choice has been made because the residual stress increased significantly when lowering the characterization temperature. This leads to the impression that the residual stress no longer consists of dry fiber contacts only, but also a contribution by local crystallization is adding to this residual stress. The increase in residual stress indicates FIC since the material must have solidified to some extent otherwise the stress would relax toward zero after the measurement. On locations where the local shear rate is high enough, FIC could occur in the neat matrix material. If this is the case, this particular stress contribution can no longer be assumed constant throughout the test, making it incorrect to subtract the residual stress from the peak and steady state shear stress. At the temperatures where the residual stress increased significantly, the friction curves are observed to be bumpy rather than smooth curves. This behavior is not visible in the friction curves at elevated temperatures with high sliding velocity, which is another indication that a mechanism becomes active at low temperatures, that is not present during friction characterization at high temperatures.

When looking at the results of the FIC experiments given in Figure 5.7, the observation can be made that the measured phase shift angle of the baseline measurement also decreases with time. This contradicts the DSC test where no crystallization has been seen during an isothermal period of six hours at 300 °C. Besides this, the phase shift angle does indeed decline faster after imposing shear rates to the sample, but no clear relation with the magnitude of this shear rate can be seen. This suggests that the used experimental method may have been unsuitable. But even though FIC has not been proved in an experimental setting, this does not mean that it is impossible to occur during friction characterization. As was explained in Chapter 4, a matrix interlayer is present between the two plies slipping across each other. The thickness of this matrix interlayer can be very low in specific locations. This implies that the shear rate is locally much higher than the average shear rate. This is also much higher than the maximum shear rate possible in the rheometer setup used for the FIC experiments. Such a high shear rate leads to a significant increase in the specific work by shear flow. According to Equation 2.3, the total specific work is proportional to the shear rate squared. Consequently, it is possible that local FIC occurs during friction characterization as it can be directly linked to the applied specific work [46, 47, 48, 56]. Further research is required to investigate the phenomenon of FIC in thermoplastic composites. A few recommendations for this are given in Section 7.1.

6.1.5. Modeling

Three different modeling approaches have been presented together with the experimental results in Section 5.6. The main observations, their causes and their consequences will be discussed here.

The friction behavior prediction obtained with the equivalent film thickness (Figure 5.13) does not represent a realistic situation as can be seen by the overprediction of the steady state shear stress at relatively low sliding velocities. Besides this, the clear kink in the curve for the steady state shear stress does not represent the gradual transition from the peak towards steady state shear stress visible in the friction curves displayed in Figure 5.6. This kink is caused by the nature of the model. Because a uniform matrix interlayer thickness has been used, the average shear stress is equal in the entire width direction of the ply-ply slip interface. This means that with increasing the sliding velocity, the critical shear stress for the onset of wall slip is achieved abruptly across the entire width of the interface. This leads to an instantaneous transition from no wall slip to full wall slip at the corresponding critical shear stress of 55 kPa. It is therefore not wise to use this model to predict the steady state shear stress response. It does however give a proper indication of the peak shear stress obtained during friction characterization and the approach can support in reducing computation time due to its simplicity.

In the model by Pierik et al. [20], the prediction of the peak shear stress is fully based on viscous shear stress in the matrix interlayer. This can be the cause for the overprediction of the peak shear stress visible at high sliding velocities in Figure 5.14. Likely, wall slip is already occurring to a small degree at high velocities during the peak behavior. This would cause a slight decrease in peak shear stress in the experimental results, which would explain the overprediction at high velocities. Compared to the prediction by using an equivalent film thickness, the steady state shear stress does not have a kink in the curve but a smooth increase towards the critical shear stress plateau. This is a more representative transition when looking at the experimentally obtained friction curves displayed in Figure 5.6.

The accuracy of the prediction is approximately equal when using fiber distributions generated by the algorithm of Melro et al. [52] or by the Darts algorithm. However, the error bars visible in Figure 5.14 and Figure 5.15 are different in size. This is caused by higher deviations between individual fiber distributions generated with the Darts algorithm. This leads to higher scattering of the shear stress prediction as this is an average of the outcome from 10 different fiber distributions.

Another difference between the results of the two different models is the difference in predicted peak and steady state shear stress at relatively low velocities. In Figure 5.14, the peak and steady state shear stress converge for relatively low sliding velocities while the curves remain parallel to each other in Figure 5.15. The latter is not in line with the experimental results at relatively high temperatures where there is no distinctive peak behavior for low sliding velocities. However, at low temperatures, this peak behavior does occur at low velocities, as can be seen in Figure 5.6. So in particular for lower temperatures, the Darts algorithm might provide more accurate results at low sliding velocities.

Also at higher sliding velocities, the Darts algorithm appears to outperform the other two models. A more extensive study with different materials and even lower sliding velocities is needed to verify this observation. If the model outcome turns out to be valid for other materials indeed, the Darts algorithm could be of great value in the prediction of the peak or steady state shear stress at low temperatures. Hence the predictive model by Pierik et al. could be applied in forming simulation software for a broader temperature range.

The predictive models by using Melro distributions or the Darts algorithm both underpredict the peak shear stress for low sliding velocities at 300 °C (see Figure A.8 and Figure A.9). The prediction of the peak shear stress is fully based on viscous shear stress. The fact that the models underpredict the actual peak shear stress at such a low temperature, indicates that an extra mechanism is active at low temperatures that increases the measured shear stress. This could be the earlier discussed FIC. If the polymer starts to solidify on a local scale because of enhanced crystallization kinetics, this could increase the measured shear stress during friction characterization and it would explain the underprediction by both of the models. However, this is not in line with the correct prediction of the peak at higher sliding velocities. According to Equation 2.3, the specific work is increased for higher shear rates [46,

47, 48, 56]. This would mean that FIC would become more dominant at higher shear rates, and thus one would expect an even bigger deviation rather than a higher resemblance.

6.2. Robustness of the research

In this section, the general robustness of the research will be discussed. Issues will be treated separately and their influence on the results will be explained.

6.2.1. Degradation

When heating thermoplastic polymers to a temperature significantly higher than their melting temperature, there is a risk of (thermal) degradation [59, 60]. To prevent this during the rheological experiments, the rheometer furnace is continuously flushed with nitrogen gas. For the used temperatures, this should be sufficient. This method has proved itself by repeated frequency sweeps with the same sample. The obtained complex viscosity proved constant, indicating that degradation is not an issue for the specific time frame.

A precaution like atmosphere control has not been present in the friction characterization setup. This would be a problem for experiments with a relatively long duration. In general, a sample in the friction characterization setup is at an elevated temperature for a duration of 5 to 15 minutes. Samples characterized at different temperatures are first heated to 365 $^{\circ}$C and then cooled to the characterization temperature. Leading to different durations at high temperatures. After all, the cooling rate in the used setup is only 7 $^{\circ}\mathrm{C}/\mathrm{min}$. According to literature, the duration of exposure to air and high temperature on the scale of the friction characterization experiments, only leads to negligible thermal degradation [59, 61]. Although, it must be stated that referred papers have described the thermal degradation of PEEK rather than LM-PAEK. It is assumed that the effects are similar, after scaling temperatures to the specific melting temperatures.

6.2.2. Viscosity curves

Continuous curves are obtained from the viscosity data by using a Cross model fit [37]. However, when applying a rheological model and calculating the viscosity at relatively high shear rates, one is extrapolating the data. It would be a better method to use a capillary rheometer as this setup is more suitable to obtain rheological material properties at relatively high shear rates. In other research, it appears that the data from a capillary rheometer does in fact overlap with the Cross model extrapolation data for this specific material [36].

6.2.3. Model comparison

In Figure 5.5, the obtained viscosity curves have a certain error margin. This error originates from the fact that the curves are averages of three individual data points from separate experiments. This error has not been taken into account when constructing the error bars in the results of the models given in Figure 5.14 and Figure 5.15. The reason for this is that the error of the models needs to be compared as well. When the error by viscosity would be included, comparing the error induced by the model itself would become more complex.

6.2.4. Time-temperature-superposition principle applied to ply-ply friction

The method of constructing a master curve at a reference temperature using the TTS principle has been used in this research to predict the slope of the friction curves during the peak-to-steady-state transition. The application of this method makes it possible to predict the duration of the peak-to-steady-state transition with respect to sliding velocity and temperature. This approach has not been used before in the field of ply-ply friction in composites. It would therefore be wise to validate this method with other combinations of fiber and thermoplastic matrix material. If the method also proves valid for other materials, it can be of value in the prediction of the friction response and thus in forming simulations of hot press forming of UD thermoplastic composite laminates.

From Figure 5.12b it becomes clear that the Arrhenius fit to the shift factor (a_{T}) is acceptable but the

data point at 300 °C ($\frac{1}{573}$ K^{-1}) is deviating. 300 °C is below the melting point of the thermoplastic matrix material. The deviation is likely caused by local FIC in the material as was explained in Section 6.1. If the material is crystallized locally, preventing the flow of matrix material, the TTS principle could possibly still be applied but the Arrhenius fit parameters obtained at higher temperatures will not be applicable anymore. This method is based on the time-dependent behavior of rheological properties but these properties undergo a severe transition when the material crystallizes, leading to an error in the Arrhenius fit for the shift factor.

7

Conclusion

After the literature review study, several gaps have been identified. Knowledge about the friction behavior of UD thermoplastic composites at significantly lower temperatures than the processing temperatures is lacking. Also, the influence on the friction behavior by the temperature effects in the neat matrix material is unknown. Crystallization, either natural or induced by flow, has not yet been investigated in combination with ply-ply friction. Modeling efforts from earlier research have not yet been compared and used at lower temperatures. According to the performed research outlined in this report, several conclusions can be formulated:

- The typical friction response consists of a shear stress overshoot during start-up, gradually reducing towards a steady state shear stress response. At typical processing temperatures, specific behavior corresponding to a certain sliding velocity is seen. It is observed that this behavior shifts to lower velocities when the temperature is lowered. This is most obvious when looking at the ratio of the peak shear stress versus the steady state shear stress for different temperatures and velocities. But this shift is also visible in the slope of the friction curves during the transition of peak shear stress towards steady state shear stress.
- Clear indications of FIC have been found during friction characterization at temperatures around and below the melting point of the thermoplastic matrix material. Attempts to prove the presence of FIC in the material have not led to plain results. Further research is required to investigate FIC during ply-ply slip of UD thermoplastic composites. Isothermal crystallization during experimental friction characterization, regardless of shear flow, has been excluded in the research.
- The modeling efforts by Pierik et al. have been compared to the obtained experimental results. A slight overprediction of the peak shear stress observed at typical processing temperatures was reduced when decreasing the temperature. The scattering of the modeling results remained approximately the same. A new algorithm to generate fiber distributions has been developed, it has proved more accurate at lower temperatures compared to two models from literature. However, a larger scatter in modeling results is observed with the new algorithm. In order to confirm its validity at lower temperatures, a more extensive study with multiple materials has to be conducted.
- A novel method, using existing predictive models and the TTS principle, has been found to predict the duration of the transition of the peak towards steady state shear stress in the friction response. This can be applied in a continuous range of sliding velocities and temperatures. If validated with other materials, this method can be of high value in improving the accuracy of hot press forming simulations of UD thermoplastic laminates.

7.1. Recommendations

Several recommendations can be given regarding future research in the field of ply-ply friction in thermoplastic UD composites. The most important one is the investigation of different materials. Where LM-PAEK or other members of the PAEK family of thermoplastics have a great future perspective regarding application in the aerospace industry for numerous reasons [62]. It is important to validate observations and statements with other thermoplastic matrix materials by performing experiments and comparing the behavior and the modeling accuracy.

Another recommendation for future research is to investigate the influence of fiber angle at lower temperatures. In the currently used friction characterization setup it has not been possible to orientate the plies different from an angle of 0 degrees. However, the influence of fiber angle can be different at lower temperatures compared to higher temperatures. With a more viscous matrix material, it is expected that fibers can move less freely in the material possibly causing different friction behavior.

As was explained in the results using Figure 5.15, the Darts algorithm combined with the approach by Pierik et al.[20] seems to predict a distinctive peak at very low velocities at low temperatures. This peak behavior is in line with other results, but with extra experiments at lower velocities, it can be experimentally validated whether this is true. At one point, the peak behavior will also disappear at low temperatures but from the current research it is not known at which sliding velocity this will happen.

The currently used method to show FIC by monitoring the evolution of the phase shift angle and storage modulus after a period of constant shear has not proved successful. In literature, a different method is proposed. Wide angle X-ray diffraction (WA-XRD) can be used to prove a specific orientation of the formed crystals during cooling [63, 64]. If they are all oriented in the same direction, this is a clear indication that they are formed after the alignment of the polymer chains has taken place. An approach to use WA-XRD to show longitudinally oriented structures in the friction characterization samples can be compiled in future research. If this proves successful, it might also be applicable to actual parts produced with hot press forming.

Cross sections have been studied with scanning electron microscopy (SEM) in this research, in an attempt to show that the polymer has obtained a different structure at the slip interface during friction characterization at 300 °C. Before the samples are loaded in the SEM, the surface has been etched using the method by Olley et al. [65]. However, the used method did not give satisfactory results because the structure of the formed crystals was not visible at all. In future research, different etching methods in combination with SEM could be used to image the structure on the slip surfaces of friction characterization samples. This could lead to more insights regarding FIC during experimental friction characterization.

References

[1] P.D. Mangalgiri. “Composite materials for aerospace applications”. In: *Bulletin of Materials Science* 22.3 (1999), pp. 657–664.

[2] P. Jerome. “Composite materials in the airbus A380-from history to future”. In: *Proceedings of the 13th International Conference on Composite Materials (ICCM-13), Beijing, China*. 2001, pp. 25–29.

[3] S.J. Pickering. “Recycling technologies for thermoset composite materials—current status”. In: *Composites Part A: applied science and manufacturing* 37.8 (2006), pp. 1206–1215.

[4] S.G. Advani, T.S. creasy, and S.F. Shuler. “Chapter 8 Rheology of long fiber-reinforced composites in sheetforming”. In: *Composite Materials Series*. Vol. 11. Elsevier, 1997, pp. 323–369. ISBN: 978-0-444-82641-1.

[5] U. Sachs. “Friction and bending in thermoplastic composites forming processes”. PhD thesis. University of Twente, Dec. 2014. ISBN: 9789462594838.

[6] A.R. Offringa. “Thermoplastic composites—rapid processing applications”. In: *Composites Part A: Applied Science and Manufacturing* 27.4 (1996), pp. 329–336.

[7] Z. Qureshi, T. Swait, R. Scaife, and H.M. El-Dessouky. “In situ consolidation of thermoplastic prepreg tape using automated tape placement technology: Potential and possibilities”. In: *Composites Part B: Engineering* 66 (2014), pp. 255–267.

[8] J.L. Gorczyca-Cole, J.A. Sherwood, and J. Chen. “A friction model for thermostamping commingled glass–polypropylene woven fabrics”. In: *Composites Part A: Applied Science and Manufacturing* 38.2 (Feb. 2007), pp. 393–406. ISSN: 1359835X.

[9] F. Saraiva. “Development of press forming techniques for thermoplastic composites”. PhD thesis. Technische Universiteit Delft, Mar. 2017.

[10] D. Tatsuno, T. Yoneyama, K. Kawamoto, and M. Okamoto. “Hot press forming of thermoplastic CFRP sheets”. In: *Procedia Manufacturing* 15 (2018), pp. 1730–1737. ISSN: 23519789.

[11] R.H.W. ten Thije and R. Akkerman. “Design of an experimental setup to measure tool-ply and ply-ply friction in thermoplastic laminates”. In: *International Journal of Material Forming* 2.1 (Dec. 2009), p. 197. ISSN: 1960-6214.

[12] C González, JJ Vilatela, JM Molina-Aldareguía, CS Lopes, and J LLorca. “Structural composites for multifunctional applications: Current challenges and future trends”. In: *Progress in Materials Science* 89 (2017), pp. 194–251.

[13] Aniform Engineering B.V. *Aniform*. 2022. URL: `https://aniform.com/`.

[14] S. Haanappel. “Forming of UD fibre reinforced thermoplastics : a critical evaluation of intra-ply shear”. PhD thesis. University of Twente, Apr. 2013. ISBN: 9789036535014.

[15] D. Dörr, M. Faisst, T. Joppich, C. Poppe, F. Henning, and L. Kärger. “Modelling approach for anisotropic inter-ply slippage in finite element forming simulation of thermoplastic UD-tapes”. In: *AIP Conference Proceedings*. Vol. 1960. 1. AIP Publishing LLC. 2018, p. 020005.

[16] J.L. Gorczyca-cole, J.A. Sherwood, L. Liu, and J. Chen. “Modeling of Friction and Shear in Thermostamping of Composites - Part I”. In: *Journal of Composite Materials* 38.21 (Nov. 2004), pp. 1911–1929. ISSN: 0021-9983.

[17] G. Lebrun, M. N. Bureau, and J. Denault. “Thermoforming-Stamping of Continuous Glass Fiber/Polypropylene Composites: Interlaminar and Tool–Laminate Shear Properties”. In: *Journal of Thermoplastic Composite Materials* 17.2 (Mar. 2004), pp. 137–165. ISSN: 0892-7057, 1530-7980.

[18] S.R. Morris and C.T. Sun. “An investigation of interply slip behaviour in AS4/PEEK at forming temperatures”. In: *Composites Manufacturing* 5.4 (Dec. 1994), pp. 217–224. ISSN: 09567143.

[19] A.M. Murtagh, J.J. Lennon, and P.J. Mallon. “Surface friction effects related to pressforming of continuous fibre thermoplastic composites”. In: *Composites Manufacturing* 6.3–4 (Jan. 1995), pp. 169–175. ISSN: 09567143.

[20] E.R. Pierik, W.J.B. Grouve, S. Wijskamp, and R. Akkerman. “On the prediction of the ply-ply friction characteristics of UD fiber-reinforced thermoplastics in melt”. In: (2021 - Ongoing, to be submitted), p. 45.

[21] E.R. Pierik, W.J.B. Grouve, S. Wijskamp, and R. Akkerman. “On the origin of start-up effects in ply-ply friction for UD fiber-reinforced thermoplastics in melt”. In: *ESAFORM 2021* (Apr. 2021).

[22] R. Scherer and K. Friedrich. “Inter- and intraply-slip flow processes during thermoforming of cf/pp-laminates”. In: *Composites Manufacturing* 2.2 (Jan. 1991), pp. 92–96. ISSN: 0956-7143.

[23] D. Zhang, D. Heider, S.G. Advani, and J.W. Gillespie. “Out of autoclave consolidation of voids in continuous fiber reinforced thermoplastic composites”. In: *SAMPE 2013* (2013), p. 16.

[24] S. Roychowdhury and S.G. Advani. “An experimental investigation of consolidation in thermoplastic filament winding”. In: *Composites Manufacturing* 2.2 (1991), pp. 97–104. ISSN: 0956-7143.

[25] H.E.N. Bersee and A. Beukers. “Consolidation of Thermoplastic Composites”. In: *Journal of Thermoplastic Composite Materials* 16.5 (2003), pp. 433–455.

[26] E.T.M. Krämer. “The formation of fiber waviness during thermoplastic composite laminate consolidation”. PhD thesis. Enschede, The Netherlands: University of Twente, 2021. ISBN: 9789036552738.

[27] *Processing guidelines for TC1225 LMPAEK composites*. Toray Advanced Composites. Dec. 2021.

[28] T. Slange, L.L. Warnet, W.J.B. Grouve, and R. Akkerman. “Influence of preconsolidation on consolidation quality after stamp forming of C/PEEK composites”. In: vol. 1769. Oct. 2016, p. 170022.

[29] D. Brands, W.J.B. Grouve, S. Wijskamp, and R. Akkerman. “Intra-ply shear characterization of unidirectional fiber reinforced thermoplastic tape using the bias extension method”. In: (2021).

[30] P.J. Mallon and C.M. Óbrádaigh. “Compliant Mold Techniques for Thermoplastic Composites”. In: *Comprehensive Composite Materials*. Elsevier, 2000, pp. 873–913. ISBN: 978-0-08-042993-9.

[31] E.R. Pierik, J. Liddiard, W.J.B. Grouve, S. Wijskamp, and R. Akkerman. “On the effect of release agent and heating time on tool-ply friction of thermoplastic composite in melt”. In: (2021), p. 8.

[32] D.J. Groves. “A characterization of shear flow in continuous fibre thermoplastic laminates”. In: *Composites* 20.1 (Jan. 1989), pp. 28–32. ISSN: 00104361.

[33] E. Pennestrì, V. Rossi, P. Salvini, and P. P. Valentini. “Review and comparison of dry friction force models”. In: *Nonlinear dynamics* 83.4 (2016), pp. 1785–1801.

[34] R.H.W. ten Thije, R. Akkerman, M. Ubbink, and L. van der Meer. “A lubrication approach to friction in thermoplastic composites forming processes”. In: *Composites Part A: Applied Science and Manufacturing* 42.8 (Aug. 2011), pp. 950–960. ISSN: 1359-835X.

[35] A.M. Murtagh and P.J. Mallon. “Chapter 5 Characterisation of shearing and frictional behaviour during sheet forming”. In: *Composite Materials Series*. Vol. 11. Elsevier, 1997, pp. 163–216. ISBN: 978-0-444-82641-1.

[36] E.R. Pierik, W.J.B. Grouve, S. Wijskamp, and R. Akkerman. “Prediction of the ply-ply friction characteristics for UD C/PAEK tapes with temperature and pressure effects”. en. In: (2022 - Ongoing, to be submitted), p. 48.

[37] T. Osswald. *Polymer Rheology: Fundamentals and Applications*. 2015th ed. Hanser Publishers.

[38] T.G. Donderwinkel. “Thermal effects during the stamp forming process”. University of Twente, July 2015, p. 120.

[39] C.W. Macosko and R.G. Larson. *Rheology: Principles, Measurements, and Applications*. Advances in interfacial engineering series. VCH, 1994. ISBN: 978-1-56081-579-2.

[40] A. Amiri, N. Hosseini, and C.A. Ulven. “Long-term creep behavior of flax/vinyl ester composites using time-temperature superposition principle”. In: *Journal of Renewable Materials* 3.3 (2015), pp. 224–233.

[41] N. Nosrati, A. Zabett, and S. Sahebian. “Long-term creep behaviour of E-glass/epoxy composite: time-temperature superposition principle”. In: *Plastics, Rubber and Composites* 49.6 (2020), pp. 254–262.

[42] M.L. Williams, R.F. Landel, and J.D. Ferry. “The temperature dependence of relaxation mechanisms in amorphous polymers and other glass-forming liquids”. In: *Journal of the American Chemical society* 77.14 (1955), pp. 3701–3707.

[43] M. Peleg, M.D. Normand, and M.G. Corradini. “The Arrhenius equation revisited”. In: *Critical reviews in food science and nutrition* 52.9 (2012), pp. 830–851.

[44] W. Wang, B. Wang, A. Tercjak, A.J. Müller, Z. Ma, and D. Cavallo. “Origin of transcrystallinity and nucleation kinetics in polybutene-1/fiber composites”. In: *Macromolecules* 53.20 (2020), pp. 8940–8950.

[45] C. Schick. “Differential scanning calorimetry (DSC) of semicrystalline polymers”. In: *Analytical and bioanalytical chemistry* 395.6 (2009), pp. 1589–1611.

[46] J. Housmans, R.J.A. Steenbakkers, P.C. Roozemond, G.W.M. Peters, and H.E.H. Meijer. “Saturation of pointlike nuclei and the transition to oriented structures in flow-induced crystallization of isotactic polypropylene”. In: *Macromolecules* 42.15 (2009), pp. 5728–5740.

[47] F.G. Hamad, R.H. Colby, and S.T. Milner. “Onset of flow-induced crystallization kinetics of highly isotactic polypropylene”. In: *Macromolecules* 48.11 (2015), pp. 3725–3738.

[48] J. Seo, D. Parisi, A.M. Gohn, A. Han, L. Song, Y. Liu, R.P. Schaake, A.M. Rhoades, and R.H. Colby. “Flow-induced crystallization of poly (ether ether ketone): Universal aspects of specific work revealed by corroborative rheology and x-ray scattering studies”. In: *Macromolecules* 53.22 (2020), pp. 10040–10050.

[49] A. van Beek. *Advanced Engineering Design: Lifetime Performance and Reliability*. TU Delft, 2006. ISBN: 978-90-810406-1-7.

[50] J.H. Ferziger, M. Perić, and R.L. Street. *Computational Methods for Fluid Dynamics*. Springer International Publishing, 2019. ISBN: 978-3-319-99693-6.

[51] S.G. Hatzikiriakos. “Wall slip of molten polymers”. In: *Progress in Polymer Science* 37.4 (Apr. 2012), pp. 624–643. ISSN: 00796700.

[52] A.R. Melro, P.P. Camanho, and S.T. Pinho. “Generation of random distribution of fibres in long-fibre reinforced composites”. In: *Composites Science and Technology* 68.9 (2008), pp. 2092–2102.

[53] *Datasheet CFRT composite laminates*. TORAY CETEX TC1225 PDS. V5. Toray Advanced Composites. Oct. 2020.

[54] W.P. Cox and E.H. Merz. *Rheology of Polymer Melts–A Correlation of Dynamic and Steady Flow Measurements*. ASTM International, 1959.

[55] R. Cardinaels, N.K. Reddy, and C. Clasen. “Quantifying the errors due to overfilling for Newtonian fluids in rotational rheometry”. In: *Rheologica Acta* 58.8 (2019), pp. 525–538.

[56] B. Nazari, A.M. Rhoades, R.P. Schaake, and R.H. Colby. “Flow-induced crystallization of PEEK: Isothermal crystallization kinetics and lifetime of flow-induced precursors during isothermal annealing”. In: *ACS Macro Letters* 5.7 (2016), pp. 849–853.

[57] S.G. Hatzikiriakos and J.M. Dealy. “Wall slip of molten high density polyethylene. I. Sliding plate rheometer studies”. In: *Journal of Rheology* 35.4 (1991), pp. 497–523.

[58] A.M. Murtagh, M.R. Monaghan, and P.J. Mallon. “Investigation of the interply slip process in continuous fibre thermoplastic composites”. In: *ICCM/9. Ceramic Matrix Composites and Other Systems.* 2 (1993), pp. 311–318.

[59] M. Day, T. Suprunchuk, J.D. Cooney, and D.M. Wiles. “Thermal degradation of poly (aryl-ether–ether-ketone)(PEEK): A differential scanning calorimetry study”. In: *Journal of applied polymer science* 36.5 (1988), pp. 1097–1106.

[60] M.I. Martín, F. Rodríguez-Lence, A. Güemes, A. Fernández-López, L.A. Pérez-Maqueda, and A. Perejón. “On the determination of thermal degradation effects and detection techniques for thermoplastic composites obtained by automatic lamination”. In: *Composites Part A: Applied Science and Manufacturing* 111 (2018), pp. 23–32.

[61] P. Patel, T. R. Hull, R.W. McCabe, D. Flath, J. Grasmeder, and M. Percy. “Mechanism of thermal decomposition of poly (ether ether ketone)(PEEK) from a review of decomposition studies”. In: *Polymer degradation and stability* 95.5 (2010), pp. 709–718.

[62] M. Richardson. “PEEK at 40”. In: *Aerospace Manufacturing* (Mar. 2019).

[63] C. Baig and B.J. Edwards. “Atomistic simulation of flow-induced crystallization at constant temperature”. In: *EPL (Europhysics Letters)* 89.3 (2010), p. 36003.

[64] R.H. Somani, B.S. Hsiao, A. Nogales, H. Fruitwala, S. Srinivas, and A.H. Tsou. “Structure development during shear flow induced crystallization of i-PP: in situ wide-angle X-ray diffraction study”. In: *Macromolecules* 34.17 (2001), pp. 5902–5909.

[65] R.H. Olley, D.C. Bassett, and D.J. Blundell. “Permanganic etching of PEEK”. In: *Polymer* 27.3 (1986), pp. 344–348.

A

Auxiliary figures

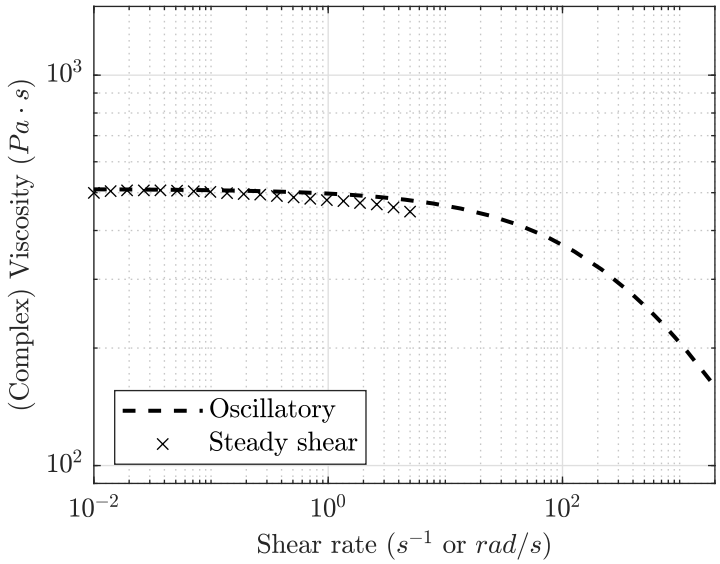

Figure A.1: Cross model fit of complex viscosity data (average of triplicate) and steady shear viscosity data (average of duplicate), at a temperature of 365 °C, together in a single figure.

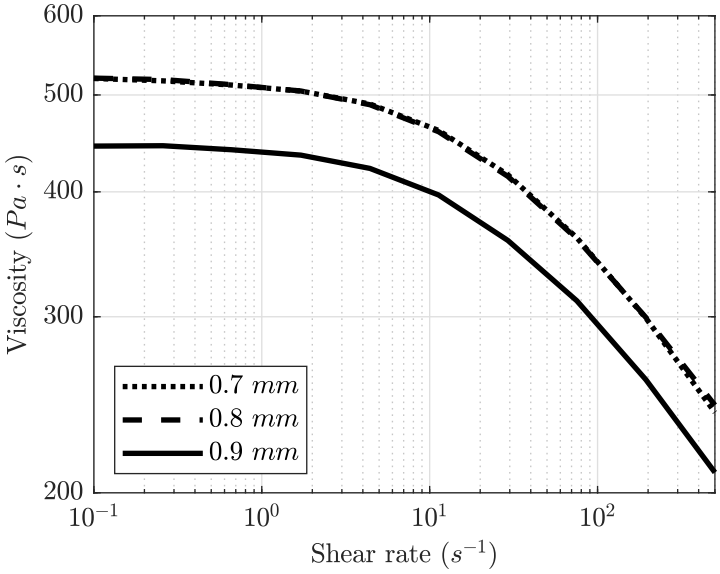

Figure A.2: Influence of gap height between the two parallel plates in a frequency sweep ranging from 0.1 to 500 rad/s with 1% strain. No influence is visible for a gap height of 0.7 and 0.8 mm as the curves overlap each other perfectly.

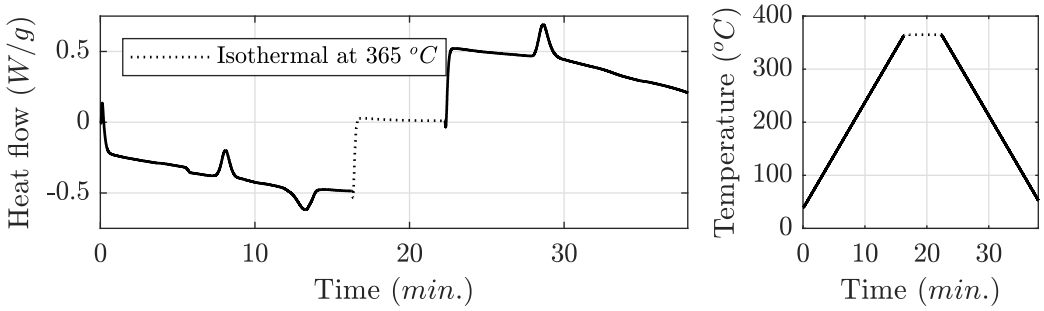

Figure A.3: DSC curve of carbon fiber reinforced LM-PAEK together with used temperature profile corresponding to a friction characterization test at 365 °C. Y-axis represents exothermic flow.

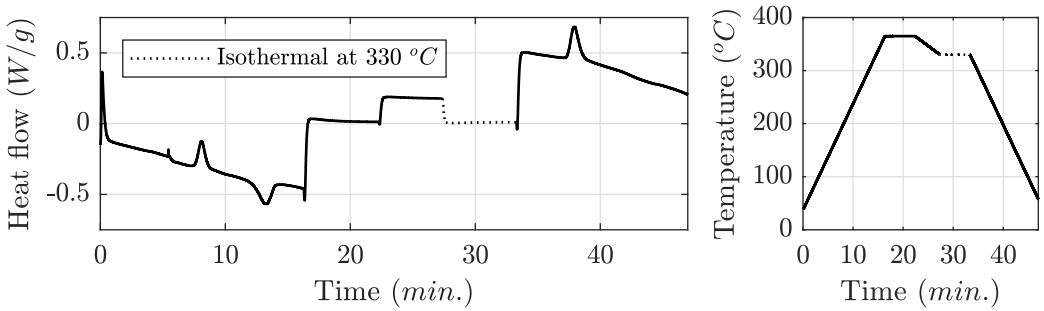

Figure A.4: DSC curve of carbon fiber reinforced LM-PAEK together with used temperature profile corresponding to a friction characterization test at 330 °C. Y-axis represents exothermic flow.

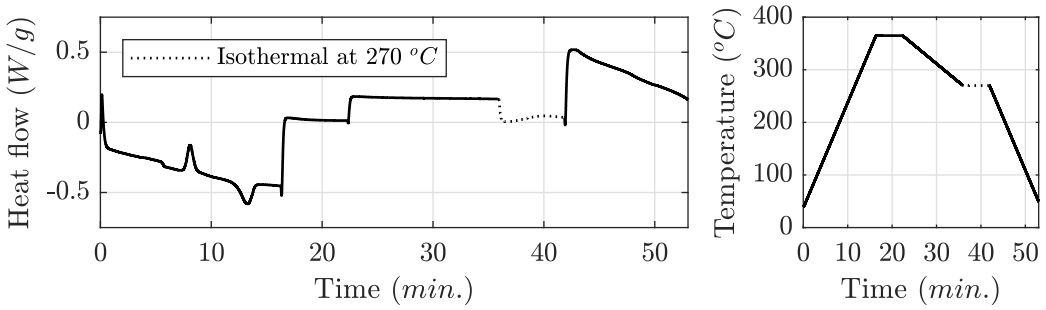

Figure A.5: DSC curve of carbon fiber reinforced LM-PAEK together with used temperature profile corresponding to a friction characterization test at 270 °C. Y-axis represents exothermic flow.

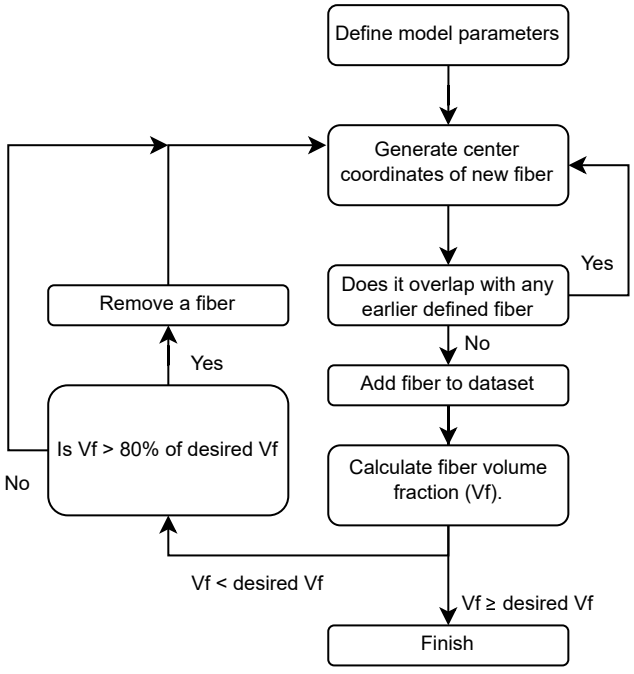

Figure A.6: Flow chart of darting algorithm to generate fiber distributions with a specific fiber volume fraction.

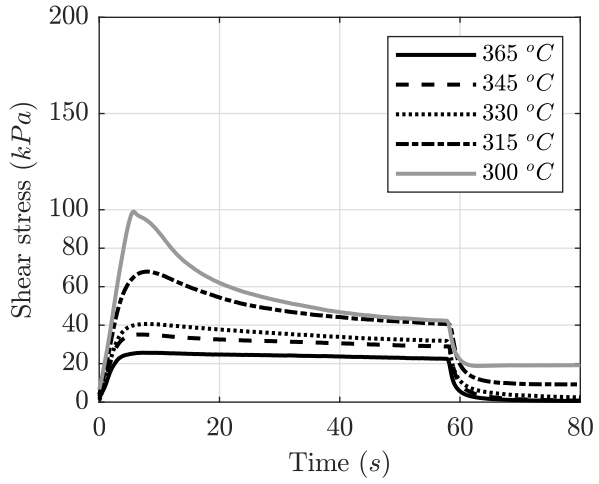

(a) Sliding velocity 10 mm/min.

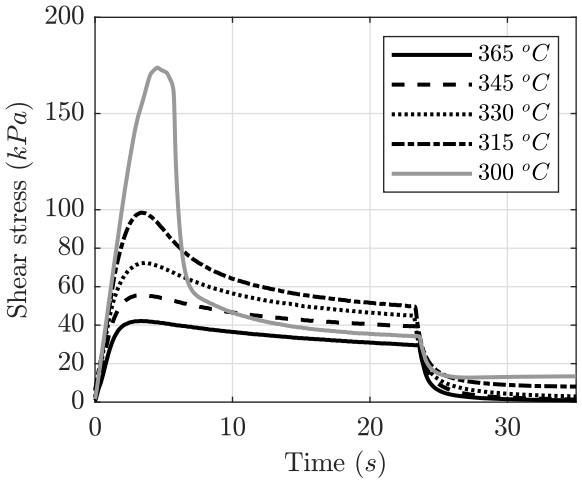

(b) Sliding velocity 25 mm/min.

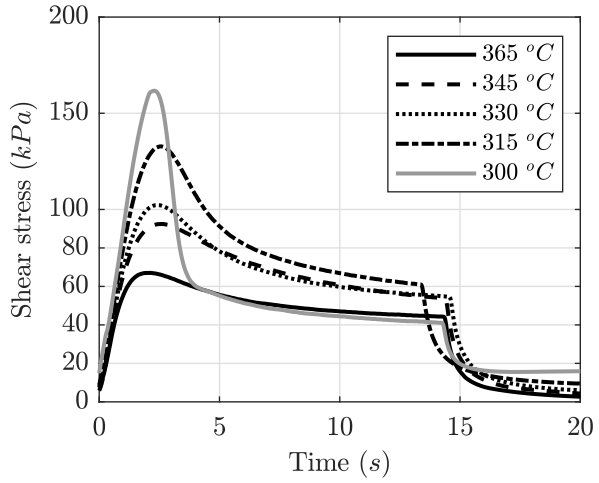

(c) Sliding velocity 40 mm/min.

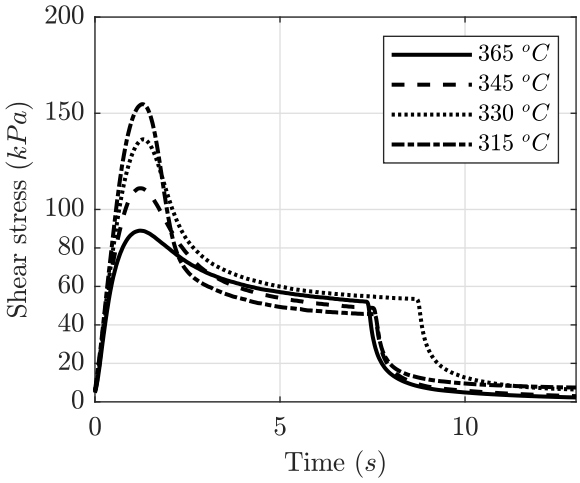

(d) Sliding velocity 75 mm/min.

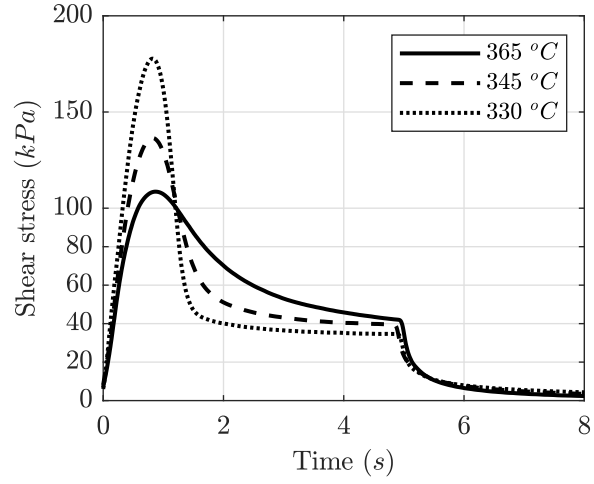

(e) Sliding velocity 125 mm/min.

Figure A.7: Results from ply-ply friction characterization versus time with varying sliding velocity and temperature. Fiber orientation is kept constant with an orientation of (0/0/0), the normal pressure has been kept constant at 15 kPa. Each curve is an average of 3 separate measurements with different samples.

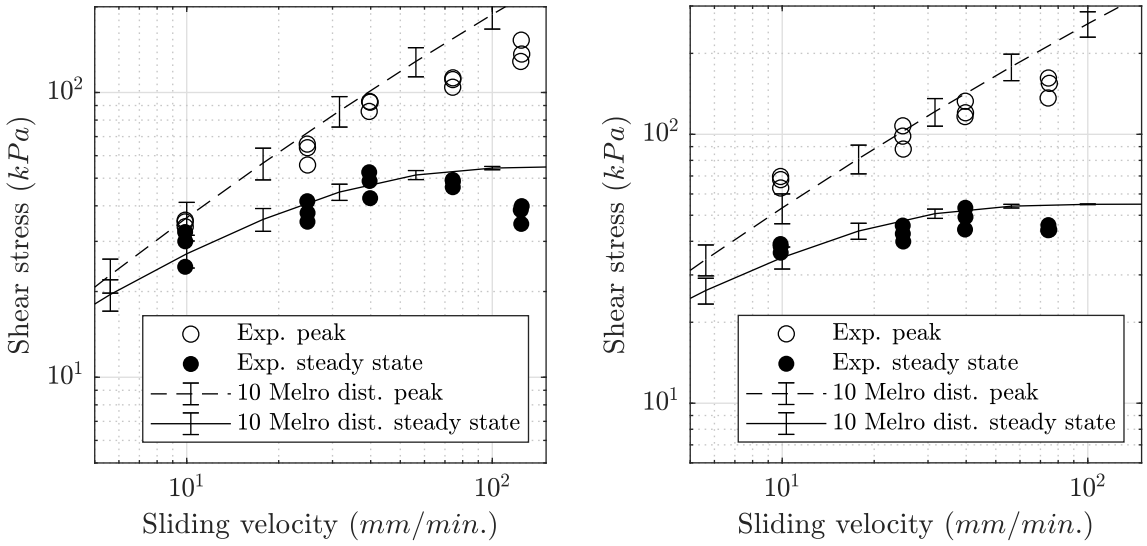

(a) 345 °C.

(b) 315 °C.

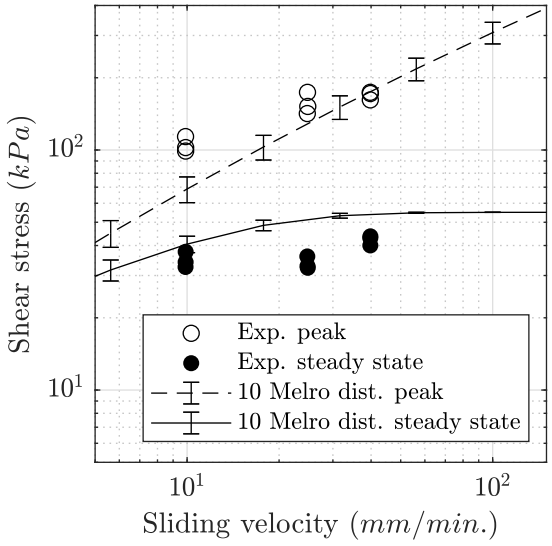

(c) 300 °C.

Figure A.8: Results from prediction of peak and steady state shear stress at 345, 315 and 345 °C by using 10 fiber distributions generated with the algorithm by Melro et al. [52].

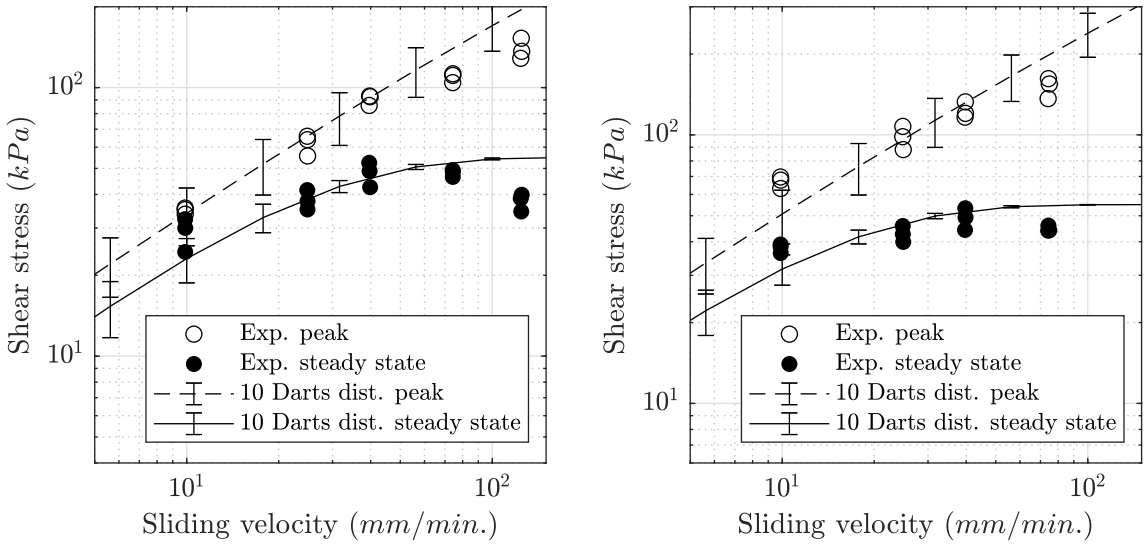

(a) 345 °C.

(b) 315 °C.

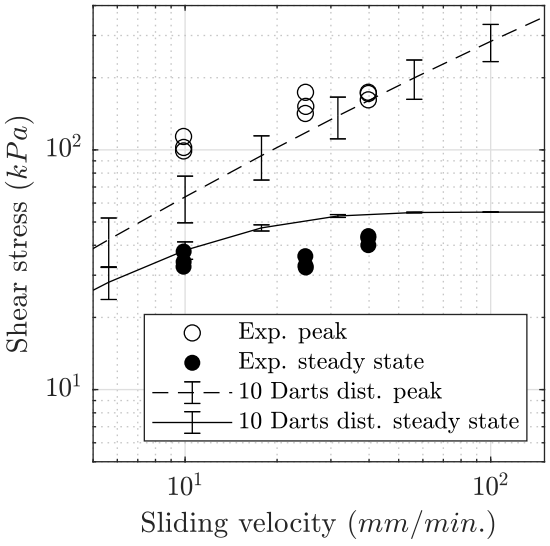

(c) 300 °C.

Figure A.9: Results from prediction of peak and steady state shear stress at 345, 315 and 300 °C by using 10 fiber distributions generated with the Darts algorithm.

B

Auxiliary tables

Table B.1: Experimental parameters of ply-ply friction characterization. Each set of parameters is utilized three times to obtain a set of data in triplicate that can be averaged to enhance the accuracy of the results.

Temperature (°C)	Sliding velocity (mm/min.)	Normal pressure (kPa)	Fiber orientation (°/°/°)
365	125 75 40 25 10	15	(0/0/0)
345	125 75 40 25 10	15	(0/0/0)
330	125 75 40 25 10	15	(0/0/0)
315	75 40 25 10	15	(0/0/0)
300	40 25 10	15	(0/0/0)